APPLICATION OF A TRACE ELEMENT FRACTIONATION MODEL TO CUMULATE GABBROIC XENOLITHS OF MAUNA KEA, HAWAII

A thesis

presented to the Faculty

of the State University of New York

at Albany

in partial fulfillment of the requirements

for the degree of

Master of Science

College of Science and Mathematics

Department of Geological Sciences

Ulrike Eberle

1990

APPLICATION OF A TRACE ELEMENT FRACTIONATION MODEL

TO

CUMULATE GABBROIC XENOLITHS OF MAUNA KEA, HAWAII

Abstract of

a thesis presented to the Faculty

of the State University of New York

at Albany

in partial fulfillment of the requirements

for the degree of

Master of Science

College of Science and Mathematics

Department of Geological Sciences

Ulrike Eberle

1990

Abstract

A trace element fractionation model originally designed to relate plutonic rocks containing a trapped glass component to a complementary volcanic rock suite was applied to olivine and opaque-oxide gabbroic xenoliths from the summit cone of Mauna Kea, Hawaii.

The mathematical model which is based on the Rayleigh Fractionation Law was extended to include the various phases present in these two groups of gabbros and was generalized to treat multiple trace elements, in this case four. These results were incorporated in a new FORTRAN program using the interval-bisection method to greatly improve the convergence time in the numerical solutions.

Calculated results of the model include the concentrations of four trace elements - Cr, Zr, Ni and Sr - in the glass phase; the weight fractions of all phases in the gabbro; the fraction of the liquid that remained in the magma chamber when some of it was trapped; and the starting compositions for Ni and Sr in the initial liquid before fractional crystallization. The choice of partition coefficients and trace element starting compositions appears to be crucial for the model results, as indicated by sensitivity calculations.

To test the model results, the glass phase in the xenoliths was analyzed for trace elements by electron microprobe. A comparison between the analyses and the values calculated by the model suggests two different possibilities for the large amount of Zr and Sr accumulating in the glass phase: Highly evolved glass might not be a true trapped liquid phase but rather was injected from the hawaiitic host during ascent to the surface. However, tiny patches of cognate melt might possibly also lead to an amplification in the amount of incompatible trace elements. A definitive solution could not be obtained by use of the model.

Acknowledgements

I am deeply indebted to Steve DeLong who introduced me to this project. He helped me with many suggestions during my study and had always an encouraging word when my motivation approached zero. This work was financially supported by his grants.

I am grateful to my committee members Steve DeLong, George Putman and Bob Kay from Cornell University for helping to improve my thesis with many good comments.

Special thanks go to Ron Fodor at North Carolina State University who kindly provided thin sections and the samples for this investigations, to Dave Wark who performed the electron-microprobe analyses at Renesselaer Polytechnical Institute and to Nobu Shimizu at Woods Hole Oceanographic Institute for analyses on the Ion-Microprobe.

I also would like to express my thanks to the University of Würzburg who made this stay here possible.

My parents and my family supported me morally and financially in an invaluable way I can never appreciate.

Thanks to everybody here in the Department of Geology who each contributed in their special way to the completion of this thesis.

For her friendship and for showing me the "American Way of Life" outside the department I am grateful to Valerie McGuire. I also want to thank all my old and new friends around the globe for companionship and caring during the last two years.

Finally, I would like to thank Jürgen for his long distance assistance and patience not only in my endless computer problems but also when I needed someone who made me "hang' in there". Thanks for friendship and love.

TABLE OF CONTENTS

LIST OF FIGURES

LIST OF TABLES

Nomenclature

C^l	- concentration of an element in the trapped liquid
C^{gab}	- concentration of an element in the gabbro
C^o	- concentration of an element in the original liquid
D	- bulk distribution coefficient
$D^{\varphi/l}$	- distribution coefficient between phase φ and the liquid
ξ	- different elements, here Cr, Ni, Sr and Zr
F	- fraction of the liquid remaining in the magma chamber when some of it was trapped
M	- relative mass fraction
ρ^{φ}	- density of phase φ
φ	- different phases, e.g. liquid(l), cpx, pl etc.
V^{φ}	- modal abundance of phase φ (in volume %)
X^{φ}	- weight fraction of each phase in the gabbro

Chapter 1

1. Introduction

The evolution of a magma chamber may be preserved in two complementary ways: 1.) by a sequence of plutonic rocks, representing crystalline phases, with or without trapped liquid, that may accumulate in proportions other than those in which they are crystallizing; and 2.) by a sequence of volcanic rocks nominally representing residual liquid. In the case of Mid-Ocean-Ridges (MOR), for example, several attempts (Miyashiro et al., 1970; Stroup et al., 1978; Tiezzi & Scott, 1980) have been made to relate gabbroic and basaltic rock suites petrogenetically, yet a definite connection could not always be substantiated. Frequently, dredged MOR Gabbros show geochemical characteristics that do not obviously relate them to basalts that were sampled at the same locations (Bloomer et al., 1989). Either sampling imprecision (DeLong & Chatelain, 1989) or different stages of tapping and further geochemical evolution of the ascending residual liquids (Tiezzi & Scott, 1980) might be significant reasons for the contrasting geochemistry of basalts and gabbros. Nevertheless, ocean-floor gabbros are generally viewed as a crystallization product of MORB magma with accumulated proportions of phases and a possible trapped liquid component (DeLong & Chatelain, 1989; Elthon, 1987; Hollister & Hopson, 1981). An evaluation of whole-rock chemistry appears to be a complex problem due to the non-uniform petrography of the rocks (Fox & Stroup, 1981). Instead, mineral chemistry provides a more useful tool for gathering information about the related liquid trend (Bloomer et al., 1989; Hodges & Papike, 1976; Tiezzi & Scott, 1980)

The classical approach to study crystallization during magmatic evolution used variations in major element oxide abundances. However, extensive observational and thermodynamic work has revealed distinct features of trace element distribution in rocks

that can be used as a helpful instrument in solving geological problems (McIntire, 1963). Properties of trace elements such as ionic radius, charge and possible ligand field stabilization are frequently quite different from the major constituents of the host phase. Due to their low concentrations, the partitioning of trace elements may result in several orders of magnitude variation during crystallization, as they exhibit strong preferences for one phase relative to the others (Wood and Fraser, 1977). All these features contribute to the fact that trace elements are sensitive indicators of igneous evolution.

In 1989, DeLong and Chatelain introduced a simple trace element mass-balance model based on the Rayleigh Fractionation Law to interrelate volcanic and plutonic rocks. The model assumes that a liquid line of descent (LLD) can be identified for which each instantaneous cumulate represents a mixture of phases +/- trapped liquid. Particularly plutonic compositions are matched with their complementary liquid by calculating the locus of a compatible-incompatible trace element pair in the magma, the mathematical details of which are developed in Chapter 2. The model predicts information on the mass-fractions of the mineral phases and any trapped liquid, the fraction of the original liquid that remained in the magma chamber when the plutonic phases crystallized and the trace element concentrations in the liquid, thus allowing some tests of the model from modal data for the plutonics and from trace element concentrations that may be measurable in any trapped liquid. A suite of cumulate gabbroic xenoliths from Mauna Kea Volcano, Hawaii, originally described by Fodor and Vandermeyden (1988), appeared to be particularly useful because these xenoliths were thought to have the necessary geological requirements for an application of the model. Fodor and Vandermeyden identified two groups of gabbros, one olivine-rich, the other with a high component of opaque oxides on the basis of petrographic and geochemical analyses and interpreted the glass phase in some of the xenoliths as trapped liquid (Fodor and Vandermeyden, 1988).

Both gabbro types can be associated petrologically with the post-shield stage alkali basalts that brought them up to the surface (Frey et al., 1990; West et al., 1988).

The primary purpose of this study is to test whether the mass-balance model of DeLong and Chatelain, (1989) can predict phase proportions and trace element contents of trapped liquid in the Mauna Kea gabbros, assuming that Fodor and Vandermeyden's petrological interpretation is correct.

Chapter 2

2. Detailed description of the model

This chapter recasts and extends the model of DeLong and Chatelain (1989) to apply it to the Mauna Kea xenoliths of Fodor and Vandermeyden (1988). They reported seven different phases in the gabbroic cumulates as will be denoted in the following equations using the abbreviations given in parentheses: a trapped liquid phase (l), clinopyroxene (cpx), olivine (ol), plagioclase (pl), chromium bearing oxides (spl), opaque oxides (opq) and apatite (ap). The unique value of Fodor and Vandermeydens sample suite is that they reported detailed modes and whole-rock analyses for major and trace elements. Among the latter, I have chosen Cr, Ni, Sr and Zr as suitable for an application of the model. An explanation for this selection is given in chapter 3.

Assuming surface equilibrium between liquid and crystal interface, the concentration of a trace element in the remaining liquid (C^l) and in the solid phase (C^φ) can be calculated with the Rayleigh Fractionation Law (Albarede, 1976):

$$C^l = C^\circ F^{D-1} \tag{1}$$

and

$$C^\varphi = D^{\varphi/l} C^\circ F^{D-1} \tag{2}$$

where C^0 is the concentration in the original liquid, F the fraction of the liquid remaining in the magma chamber when some of it was trapped, $D^{\varphi/l}$ the distribution coefficient between phase φ and the liquid, and D is the bulk distribution coefficient:

$$D = \Sigma W^\varphi D^{\varphi/l} \tag{3}$$

with W^φ being the weight fraction of each phase φ crystallizing from the liquid.

Figure 1 schematically shows the concentrations of a compatible and an incompatible element in a fractionating liquid and two cumulus phases A and B. A gabbroic mixture of the phases (A and B) and the liquid (l) must fall within the triangle defined by the dashed lines. The three hexagons represent compositions of A, B and l, respectively, in equilibrium with each other for a certain value of F. Bulk solid curves with $C^{\varphi} = D^{\varphi/l}\, C^{o}\, F^{D-1}$ reflect compositions of liquid-free cumulates if the phases accumulate in the same portions in which they crystallize.

Using Fodor and Vandermeydens data, (1988) for the cumulate gabbroic xenoliths from Mauna Kea (Table 1), I adjusted the DeLong-Chatelain model for seven phases and four elements. Thus, four statements can be derived from Eq. (1):

$$C^{l}_{Cr} = C^{o}_{Cr} F^{D_{Cr}-1} \tag{4}$$

$$C^{l}_{Zr} = C^{o}_{Zr} F^{D_{Zr}-1} \tag{5}$$

$$C^{l}_{Ni} = C^{o}_{Ni} F^{D_{Ni}-1} \tag{6}$$

$$C^{l}_{Sr} = C^{o}_{Sr} F^{D_{Sr}-1} \tag{7}$$

A combination of (4) and (5) results in

$$(C^{l}_{Cr} / C^{o}_{Cr}) = (C^{l}_{Zr} / C^{o}_{Zr})^{D^*} \tag{8}$$

where $D^* = (D_{Cr} - 1)/(D_{Zr} - 1)$.

Mass balance for all seven phases yields the following equation:

$$X^{l} + X^{cpx} + X^{ol} + X^{pl} + X^{spl} + X^{opq} + X^{ap} = 1 \tag{9}$$

with X^{φ} being the weight fraction of each phase in the gabbro and

$$C^{gab}_{Cr} = X^{l} C^{l}_{Cr} + X^{cpx} C^{cpx}_{Cr} + X^{ol} C^{ol}_{Cr} + X^{pl} C^{pl}_{Cr} + X^{spl} C^{spl}_{Cr} + X^{opq} C^{opq}_{Cr} + X^{ap} C^{ap}_{Cr}$$

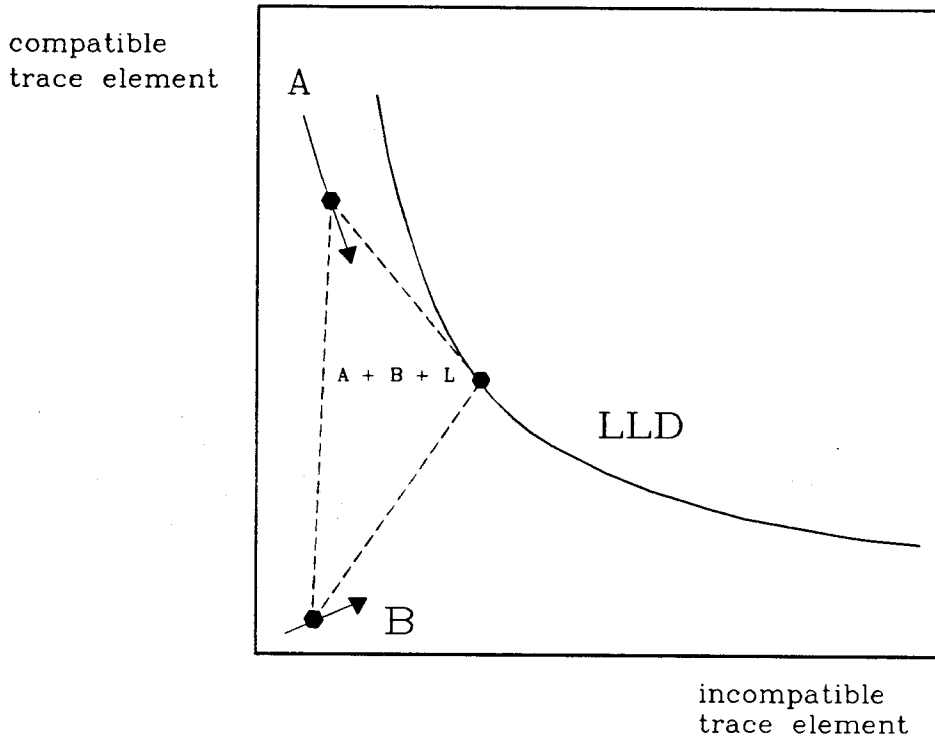

Fig. 1: Concentrations of a compatible versus an incompatible element in a fractionating liquid l and phases A and B crystallizing from it. Coexisting compositions of A, B and l are represented by hexagons. A mixture of A, B and the liquid (cumulate gabbro with a trapped liquid phase) should be located in the dashed-line triangle. Increasing degree of fractionation moves the triangle along the LLD. (after DeLong and Chatelain, 1989)

Both sides are divided by C^{l}_{Cr}, thus the concentration of Cr in the basaltic liquid can be expressed by:

$$\frac{C^{gab}_{Cr}}{C^{l}_{Cr}} = X^{l} + X^{cpx}D^{cpx/l}_{Cr} + X^{ol}D^{ol/l}_{Cr} + X^{pl}D^{pl/l}_{Cr} + X^{spl}D^{spl/l}_{Cr} + X^{opq}D^{opq/l}_{Cr} + X^{ap}D^{ap/l}_{Cr} \qquad (10)$$

The concentration of Zr, Ni and Sr are represented by the following three equations analogous to Eq. 10:

$$\frac{C^{gab}_{Zr}}{C^{l}_{Zr}} = X^{l} + X^{cpx}D^{cpx/l}_{Zr} + X^{ol}D^{ol/l}_{Zr} + X^{pl}D^{pl/l}_{Zr} + X^{spl}D^{spl/l}_{Zr} + X^{opq}D^{opq/l}_{Zr} + X^{ap}D^{ap/l}_{Zr} \qquad (11)$$

$$\frac{C^{gab}_{Ni}}{C^{l}_{Ni}} = X^{l} + X^{cpx}D^{cpx/l}_{Ni} + X^{ol}D^{ol/l}_{Ni} + X^{pl}D^{pl/l}_{Ni} + X^{spl}D^{spl/l}_{Ni} + X^{opq}D^{opq/l}_{Ni} + X^{ap}D^{ap/l}_{Ni} \qquad (12)$$

$$\frac{C^{gab}_{Sr}}{C^{l}_{Sr}} = X^{l} + X^{cpx}D^{cpx/l}_{Sr} + X^{ol}D^{ol/l}_{Sr} + X^{pl}D^{pl/}_{Sr} + X^{spl}D^{spl/l}_{Sr} + X^{opq}D^{opq/l}_{Sr} + X^{ap}D^{ap/l}_{Sr} \qquad (13)$$

An estimate of relative mass fractions of the gabbro components can be obtained by petrographical observations:

$$M_1 = \frac{X^{cpx}}{X^{pl}} = \frac{\rho^{cpx}\, V^{cpx}}{\rho^{pl}\, V^{pl}} \qquad (14)$$

$$M_2 = \frac{X^{ol}}{X^{pl}} = \frac{\rho^{ol}\, V^{ol}}{\rho^{pl}\, V^{pl}} \qquad (15)$$

$$M_3 = \frac{X^{spl}}{X^{pl}} = \frac{\rho^{spl}\, V^{spl}}{\rho^{pl}\, V^{pl}} \qquad (16)$$

$$M_4 = \frac{X^{opq}}{X^{pl}} = \frac{\rho^{opq}\, V^{opq}}{\rho^{pl}\, V^{pl}} \qquad (17)$$

$$M_5 = \frac{X^{ap}}{X^{pl}} = \frac{\rho^{ap}\, V^{ap}}{\rho^{pl}\, V^{pl}} \qquad (18)$$

with ρ^{φ} as the density of phase φ and V^{φ} as the modal abundance (in vol%).

So far, for any particular sample, there are fourteen equations (4-7, 9-18) and sixteen unknowns:

- the concentrations of Cr, Zr, Ni and Sr in the trapped liquid component (C^{l}_{Cr}, C^{l}_{Zr}, C^{l}_{Ni}, C^{l}_{Sr})
- the instantaneous fraction of original liquid (F) remaining in the magma chamber when some of it was trapped
- the mass fractions of the seven rock components (X^{l}, X^{cpx}, X^{ol}, X^{pl}, X^{spl}, X^{opq}, X^{ap}), neglecting the fact that it is not known in which phase the liquid component is masked
- and the starting compositions of the fractionation trend for Cr, Zr, Ni and Sr (C^{o}_{Cr}, C^{o}_{Zr}, C^{o}_{Ni} and C^{o}_{Sr}) in the magma.

Thus, assuming two values, most conveniently C^{o}_{Cr} and C^{o}_{Zr}, and the partition coefficients $D^{\varphi/l}_{Cr}$, $D^{\varphi/l}_{Zr}$, $D^{\varphi/l}_{Ni}$ and $D^{\varphi/l}_{Sr}$, the remaining fourteen values can be calculated.

DeLong and Chatelain noted (1989) that the configuration of the equations implies a generalizing aspect: dependent on the geological setting, an arbitrary number of elements and phases can be added by establishing suitable terms to Eq. (9-13) and Eq. (14-18). It is remarkable that each additional unknown, either element or phase, is represented by a new equation, hence, only two parental concentrations for the magma must be assumed; additional starting compositions can be calculated.

Combining Eq. (9) and (14) gives

$$X^{cpx} = \frac{M_1 (1 - X^l)}{1 + M_1 + M_2 + M_3 + M_4 + M_5} \quad (19)$$

Similarly, Eq. (9) can be combined with (15-18):

$$X^{ol} = \frac{M_2 (1 - X^l)}{1 + M_1 + M_2 + M_3 + M_4 + M_5} \quad (20)$$

$$X^{pl} = \frac{1 - X^l}{1 + M_1 + M_2 + M_3 + M_4 + M_5} \quad (21)$$

$$X^{spl} = \frac{M_3 (1 - X^l)}{1 + M_1 + M_2 + M_3 + M_4 + M_5} \quad (22)$$

$$X^{opq} = \frac{M_4 (1 - X^l)}{1 + M_1 + M_2 + M_3 + M_4 + M_5} \quad (23)$$

$$X^{ap} = \frac{M_5 (1 - X^l)}{1 + M_1 + M_2 + M_3 + M_4 + M_5} \quad (24)$$

Substitution of Eq. (19-24) into Eq. (10-13) and rearranging results in :

$$\frac{C^{gab}_{Cr}}{C^{l}_{Cr}} = (1 - \alpha_{Cr}) X^l + \alpha_{Cr} \quad (25)$$

$$\frac{C^{gab}_{Zr}}{C^{l}_{Zr}} = (1 - \alpha_{Zr}) X^l + \alpha_{Zr} \quad (26)$$

$$\frac{C^{gab}_{Ni}}{C^{l}_{Ni}} = (1 - \alpha_{Ni})\,X^{l} + \alpha_{Ni} \tag{27}$$

$$\frac{C^{gab}_{Sr}}{C^{l}_{Sr}} = (1 - \alpha_{Sr})\,X^{l} + \alpha_{Sr} \tag{28}$$

where

$$\alpha_{\xi} = \frac{M1D^{cpx/l}_{\xi} + M2D^{ol/l}_{\xi} + D^{pl/l}_{\xi} + M3D^{spl/l}_{\xi} + M4D^{opq/l}_{\xi} + M5D^{ap/l}_{\xi}}{1 + M1 + M2 + M3 + M4 + M5} \tag{29}$$

for a specific element ξ.

A combination of Eq. (25) and (26) and succeeding rearrangement leads to the elimination of X^{l}:

$$\frac{C^{gab}_{Cr}}{R1\left(\frac{C^{gab}_{Zr}}{C^{l}_{Zr}}\right) + (1 - R1)} - C^{l}_{Cr} = 0 \tag{30}$$

with $R1 = (1 - \alpha_{Cr})/(1 - \alpha_{Zr})$.

Eq. (4) is coupled with (5) resulting in

$$\frac{C^{l}_{Cr}}{C^{o}_{Cr}} = \left(\frac{C^{l}_{Zr}}{C^{o}_{Zr}}\right)^{D^{*}} \tag{31}$$

Analogous, Eq. (6) and (5) and (7) and (5) are combined:

$$\frac{C^{l}_{Ni}}{C^{o}_{Ni}} = \left(\frac{C^{l}_{Zr}}{C^{o}_{Zr}}\right)^{D^*N} \tag{32}$$

$$\frac{C^{l}_{Sr}}{C^{o}_{Sr}} = \left(\frac{C^{l}_{Zr}}{C^{o}_{Zr}}\right)^{D^*S} \tag{33}$$

where $D^*N = (D_{Ni} - 1)/(D_{Zr} - 1)$

and $D^*S = (D_{Sr} - 1)/(D_{Zr} - 1)$.

Solving Eq. (31) for C^{l}_{Cr} and substituting it into (30) gives

$$\frac{C^{gab}_{Cr}}{R1\left(\frac{C^{gab}_{Zr}}{C^{l}_{Zr}}\right) + (1 - R1)} - C^{o}_{Cr}\left(\frac{C^{l}_{Zr}}{C^{o}_{Zr}}\right)^{D^*} = 0 \tag{34}$$

In the same way, Eq. (25) and (27), as well as (25) and (28) can be combined with Eq. (31) resulting in

$$\frac{C^{gab}_{Cr}}{R2\left(\frac{C^{gab}_{Ni}}{C^{l}_{Ni}}\right) + (1 - R2)} - C^{o}_{Cr}\left(\frac{C^{l}_{Zr}}{C^{o}_{Zr}}\right)^{D^*} = 0 \tag{35}$$

and

$$\frac{C^{gab}_{Cr}}{R3\left(\frac{C^{gab}_{Sr}}{C^{l}_{Sr}}\right)+(1 - R3)} - C^{o}_{Cr}\left(\frac{C^{l}_{Zr}}{C^{o}_{Zr}}\right)^{D^*} = 0 \qquad (36)$$

where $R_i = (1 - \alpha_{Cr})/(1 - \alpha_{\xi})$

Eq. (34) can be solved numerically for C^{l}_{Zr} and this value is then used to find the other unknowns (see Appendix A for final formulas).

These relations were used to apply the model to the available data for the Mauna Kea gabbroic xenoliths (see chapter 4).

Chapter 3

3.1 Geological Setting

The gabbroic xenoliths that are the focus of this study are from the summit cone of Mauna Kea, the highest (4206m) of five major volcanoes on the island of Hawaii. The typical life-cycle of a Hawaiian volcano includes four stages of: 1.) alkalic preshield eruptives, 2.) tholeiitic shield-building lavas that comprise the largest volume of the volcano 3.) less frequent eruptions of alkalic lavas during the post-shield period and 4.) SiO2-poor lavas forming the posterosional stage (Clague & Dalrymple, 1987). The subaerial exposed rocks of Mauna Kea belong to the post-shield stage and have been divided into two stratigraphic units. The older Hamakua Lavas are mainly shield-building, moderately olivine-plagioclase-augite-phyric tholeiites to transitional alkali basalts that are exposed with ankaramites and almost aphyric high Fe-Ti basalts (Frey et al., 1990). The younger, more evolved Laupahoehoe Volcanics, cap the shield-building Hamakua lavas with a relatively thin cover of hawaiites and mugearites (West et al., 1988). This suite is essentially aphyric with rare plagioclase phenocrysts and plagioclase, olivine and magnetite microphenocrysts. The groundmass includes the same phases with an additional component of clinopyroxene. Both the scarcity of phenocrysts and the fine-grained texture indicate that the lavas likely represent liquid compositions. The summit cone of Mauna Kea in which the gabbroic xenoliths were found is part of the Laupahoehoe Volcanics.

3.2. Petrographical description of the xenoliths

Fodor and Vandermeyden (1989) identified two types of gabbros in the summit cone:

3.2.1. Olivine Gabbros

This group consists of euhedral to anhedral clinopyroxene, plagioclase, olivine, and Cr-bearing oxides (Fodor & Vandermeyden, 1988). Olivine and clinopyroxene sometimes have poikilitically enclosed plagioclase (Fig. 2) - the reverse relationship being less common - leading to the conclusion, that plagioclase and clinopyroxene crystallized approximately at the same time after Cr-spinel and olivine had been separated (Vandermeyden, 1985). Cr-spinel occurs for the most part interstitially and is rarely found as an olivine inset. Brown glass is observed in small interstitial patches (Fig. 3) and might represent magmatic liquid that was locked up by the developing cumulate pile. Veinlets of black microphyric glass that resemble the basalt host, extend into the gabbros (Fig. 4). A cumulate origin might be reflected by subparallel alignment and interference-boundaries of plagioclase crystals (Fig. 5) in samples with nearly one-half plagioclase (Vandermeyden, 1985).

3.1.2. Opaque-oxide Gabbros

Clinopyroxene, plagioclase, and Fe-Ti-oxides were described by Fodor and Vandermeyden, 1988, as major constituents. One sample (# 14) contains exceptional high clinopyroxene and a higher opaque-oxide phase content than the other specimen, indicating some kind of an accumulated character. Olivine was rarely or not at all detected. Fe-Ti-oxides are sometimes enclosed in clinopyroxene.

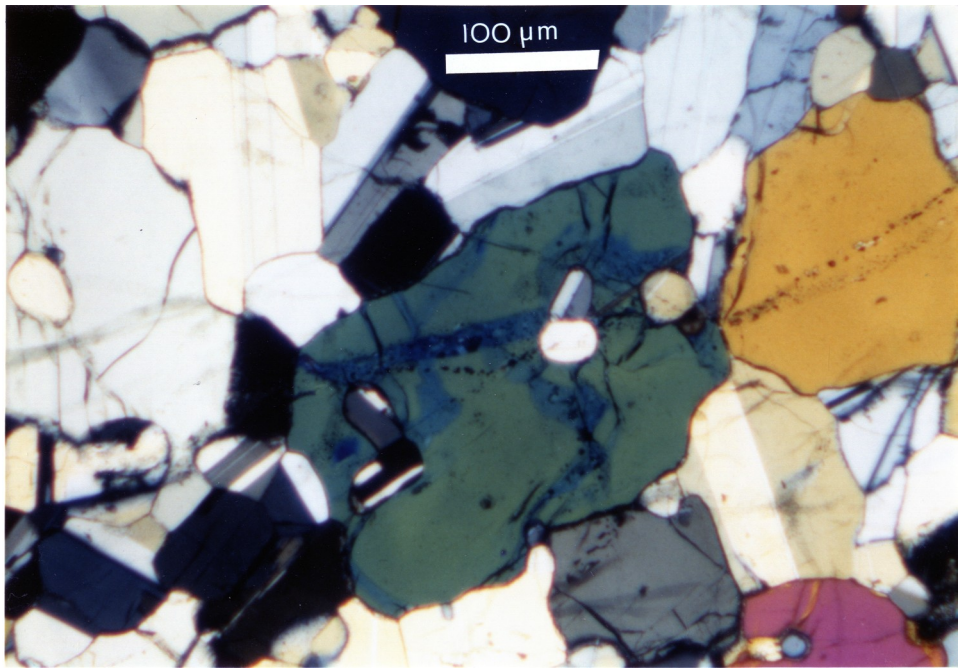

Fig. 2: Olivine poikilitically encloses plagioclase (sample #6, all samples kindly provided by R. Fodor)

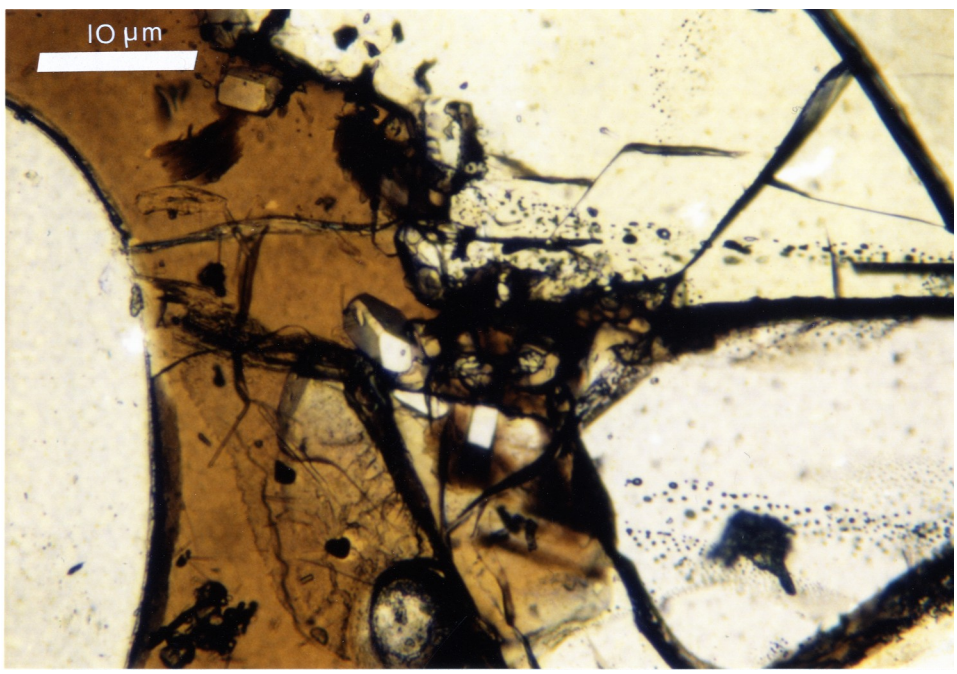

Fig. 3: Interstitial brown glass phase (sample #9)

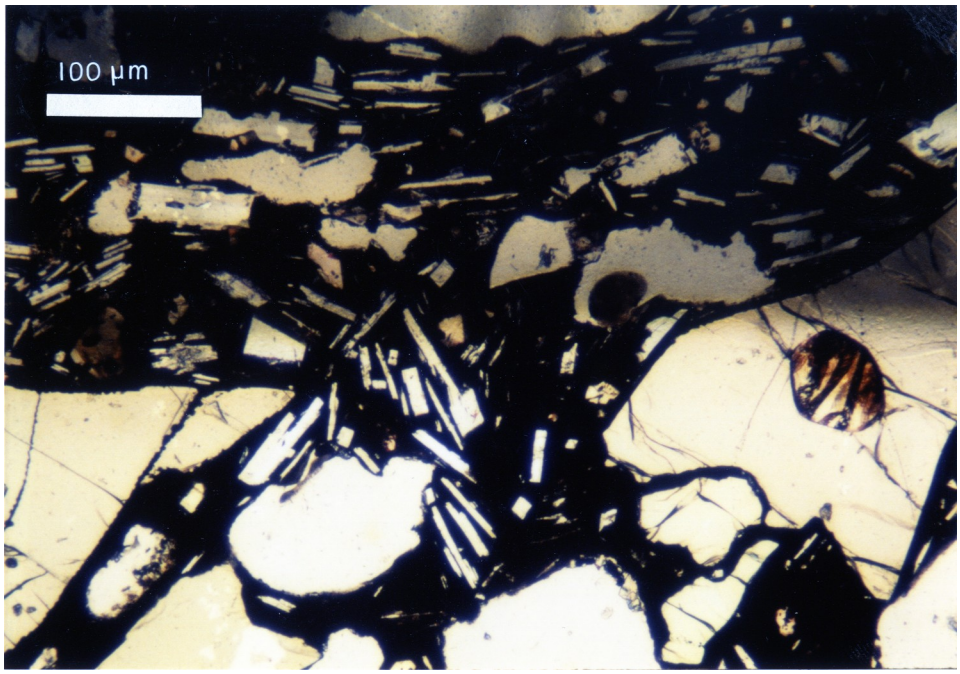

Fig. 4: Veinlets of basalt host extend into the gabbro (sample #18)

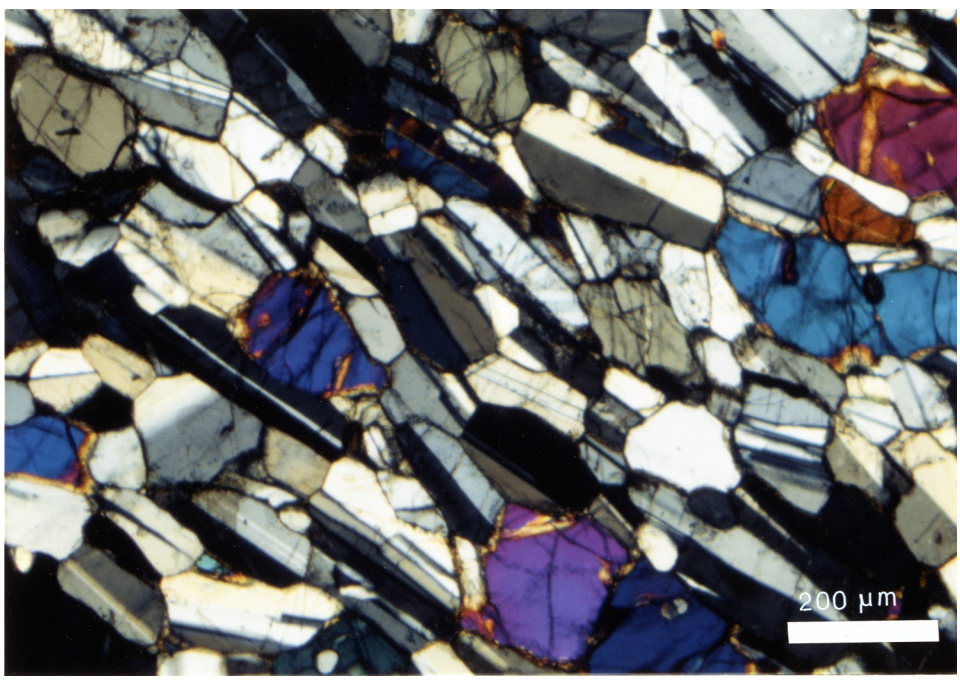

Fig. 5: Subparallel alignment of plagioclase (sample #1A)

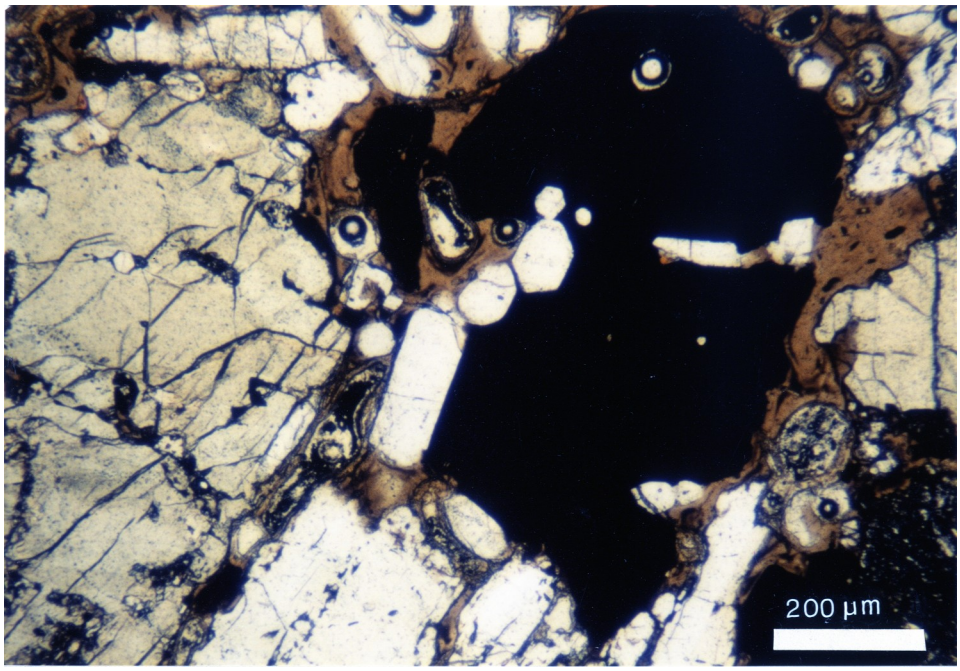

Fig. 6: Abundant apatite within and around an Fe-Ti oxide crystal, brown clear phase is interstitial glass (sample #19A)

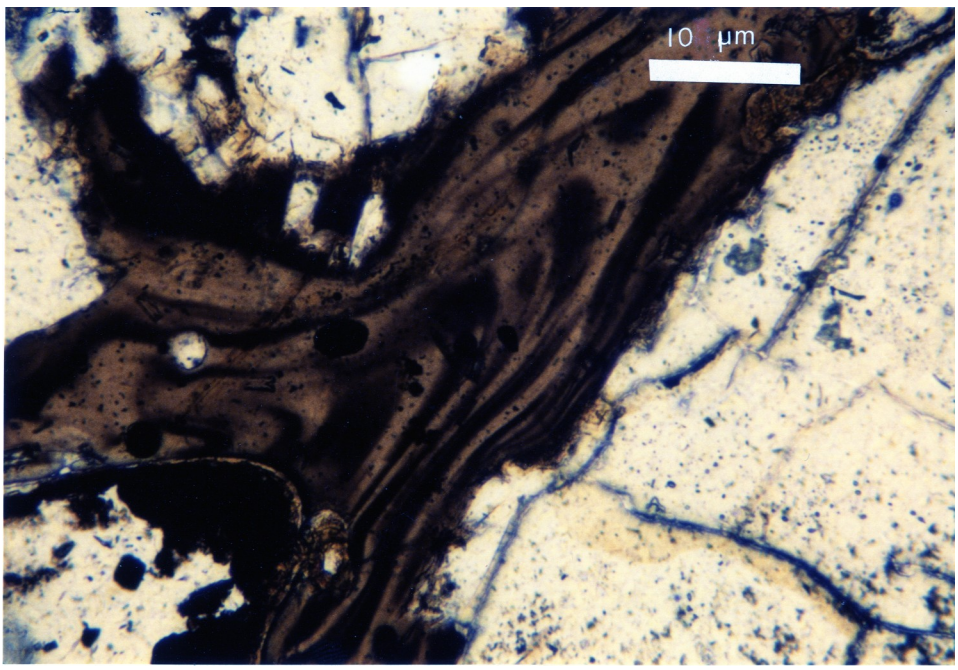

Fig. 7: Clear interstitial glass with flow structures (sample #19A)

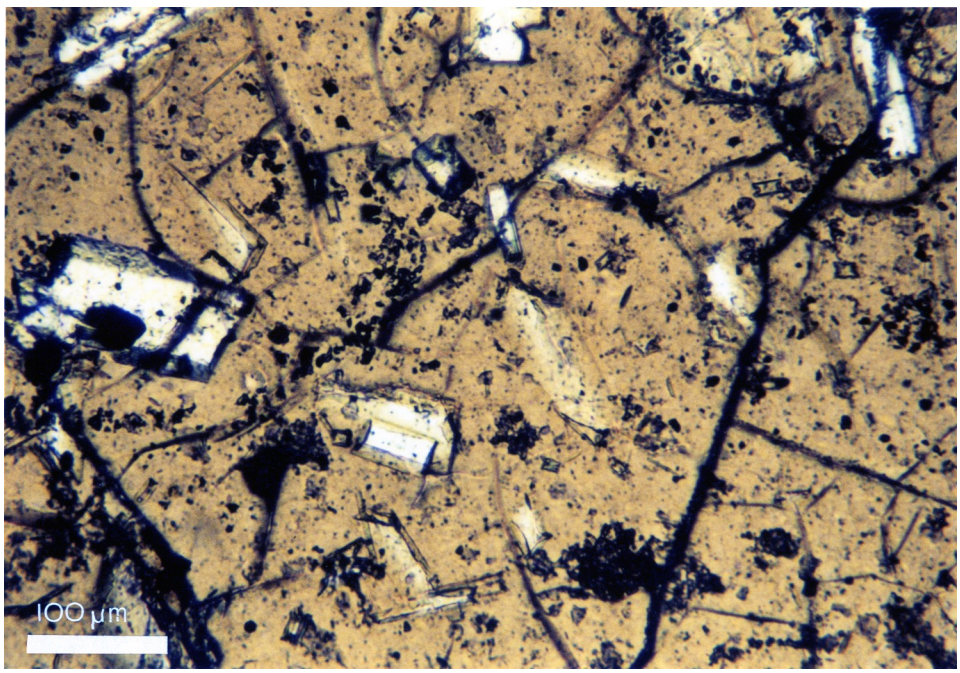

Fig. 8: Plagioclase crystallites and other impurities in brown glass (sample #13)

Around and within these oxides, abundant apatite (9 vol%) is visible in one of the samples (Fig. 6). Brown glass surrounds the oxide-phase displaying a clear image with flow structures (Fig. 7) or includes plagioclase crystallites (Fig. 8). Plagioclase shows weak cumulate lamination on a microscale that cannot be associated with the common nomenclature of cumulate rocks.

3.2 Post-shield evolution at Mauna Kea

As a prerequisite for modelling the fractionation of a magmatic liquid, it is presumed that the gabbros formed during a single magmatic event (Albarede, 1976). To support this statement, one has to gain as much evidence as possible from the surrounding geological setting. In the following part, two points of view are presented that try to give some insight into the magmatic history of Mauna Kea, i. e. into the relations of plutonic and volcanic rocks at this location.

One possible explanation for the petrogenetic evolution was given by Fodor and Vandermeyden (1988): They inferred from textural evidence of compositional layering as well as from the presence of wehrlitic and dunitic xenoliths in the summit cone, that the gabbros likely segregated in a magma chamber-like reservoir. FeO*/MgO-ratios of olivine gabbros show geochemical agreement with a derivation from a tholeiitic to a transitional alkali basalt parent that formed the shield-building lavas of Mauna Kea (MacDonald and Katsura, 1964). The low Cr- and Ni-content in olivines and pyroxenes of opaque-oxide gabbros (Table 1) corroborates the hypothesis that these rocks tend to have been crystallized from a more evolved alkali to hawaiitic suite.

Fractionation from parent- to daughter-magma (a Mg-rich alkali basalt taken as parent and a Laupahoehoe hawaiite as daughter) was estimated by least squares modelling of major elements (Fodor and Vandermeyden 1988).

TABLE I Trace element and modal data for Mauna Kea gabbroic xenoliths, analyzed by Fodor and Vandermeyden, 1988

sample	Whole-rock Concentrations (ppm)				Mode (vol%)							$M = (\rho^{*} V^{*} / \rho pl \; Vpl)$					
	Cr	Ni	Zr	Sr	ol	cpx	pl	spl	opq	ap	glass	ol	cpx	spl	opq	ap	glass
Olivine Gabbros																	
Trans. Trend																	
2A	1700	870	33	160	32.30	42.80	24.80	0.10	0	0	0	1.64	2.11	0.01	0	0	0
2B	1675	830	35	205	28.10	43.10	28.80	0	0	0	0	1.23	1.83	0	0	0	0
9	1975	670	61	180	23.70	54.90	19.70	0.60	0	0	1.10	1.51	3.41	0.05	0	0	0.15
4	2085	565	64	275	24.00	49.60	25.50	0.90	0	0	0	1.18	2.38	0.05	0	0	0
18	2800	625	54	115	20.40	68.20	7.20	0	0	0	3.20	3.57	11.58	0	0	0	1.22
1B	1930	605	63	210	19.80	53.40	23.00	3.10	0	0	0.60	1.08	2.84	0.21	0	0	0.07
8	1700	530	60	315	15.50	51.20	32.30	0	0	0	1.00	0.60	1.94	0	0	0	0.09
Hamakua Trend																	
6	1215	530	85	525	25.10	30.20	44.40	0	0	0	0.30	0.71	0.83	0	0	0	0.02
3A	1000	260	81	495	9.50	48.80	41.30	0.40	0	0	0	0.29	1.44	0.02	0	0	0
1A	880	365	95	560	7.80	40.60	51.20	0.20	0	0	0.20	0.19	0.97	0.01	0	0	0.01
3B	465	325	95	550	5.50	43.80	50.70	0	0	0	0	0.14	1.06	0	0	0	0
11	855	360	94	600	7.80	50.80	41.40	0	0	0	0	0.24	1.50	0	0	0	0
Opaque-Oxide Gabbros																	
14	15	9	106	140	0	58.0	14.80	0	27.20	0	0	0	4.79	0	3.27	0	0
17A	10	13	140	585	0	33.3	47.90	0	18.70	0	0	0	0.85	0	0.69	0	0
12	10	12	142	570	0.10	30.9	44.20	0	16.40	0	8.40	0	0.85	0	0.66	0	0.52
15B	10	10	132	575	0	33.4	47.90	0	18.50	0	0.20	0	0.85	0	0.69	0	0.01
13**	63	10	171	540	0	41.4	40.90	0	11.30	0	6.40	0	1.24	0	0.49	0	0.43
16	10	8	159	750	0	30.6	46.40	0	23.00	0	0	0	0.81	0	0.88	0	0
19A	10	12	170	780	0	23.2	50.60	0	14.40	9.10	2.70	0	0.56	0	0.51	0.21	0.15

$\rho pl=2.7$, $\rho cpx=3.3$, $\rho ol=3.4$, $\rho spl=4.2$, $\rho opq=4.8$, $\rho ap=3.2$, $\rho glass=2.75$ (densitites ρ in g/ccm)

After 60 % crystallization, including a large amount of clinopyroxene that indeed agrees with the xenoliths modal data, the parental liquid yields a hawaiitic composition similar to the Laupahoehoe hawaiite. A Hamakua basaltic and hawaiitic assemblage can be reached by 25 - 30 % crystallization. Taking the statement by Frey and his coworkers (1990) that Hamakua lavas are the residual liquids of the low-pressure fractionation of olivine, plagioclase and clinopyroxene (olivine gabbros), it is plausible to use a Hamakua basalt and a hawaiite as a daughter magma for modelling. Hamakua Volcanics and opaque-oxide gabbros cannot be directly related since the high Fe-Ti-content in the Hamakua daughter composition (Frey et al. 1989) rules out a segregation of an opaque-oxide-rich rock. Interstitial glass, assuming it is trapped magmatic liquid, was modelled by 63 % crystallization from a gabbroic assemblage.

In contrast to the once common motto, "when in doubt, settle out" (McBirney and Noyes, 1979), Fodor and Vandermeyden suggest an *in situ* solidification process for the formation of the gabbroic cumulates. Along the walls of a magma chamber, a static layer, in which the different mineral phases accumulate, interacts with convective magma currents and gradually advances from the walls of the magma chamber towards the center (McBirney and Noyes, 1979). Temperature gradients within the boundary zone might be one cause for adcumulate growth (Fodor and Vandermeyden, 1988). The residual liquid undergoes further evolution, reaching alkalic composition and eventually erupts as the Hamakua Volcanics. With continuing evolution, olivine diminishes and Fe-Ti-oxides join the crystallization and thus indicate the formation of opaque-oxide gabbros.

In summary, Fig. 9 shows a possible evolutionary path for the post-shield events at Mauna Kea. Olivine and opaque-oxide gabbros crystallized in a cooling magma chamber from a mafic alkalic parent that reached a more evolved alkalic state. While some of the liquid might have been trapped by the crystallizing cumulates, the other part possibly erupted at the surface as Hamakua Volcanics. New magma of hawaiitic

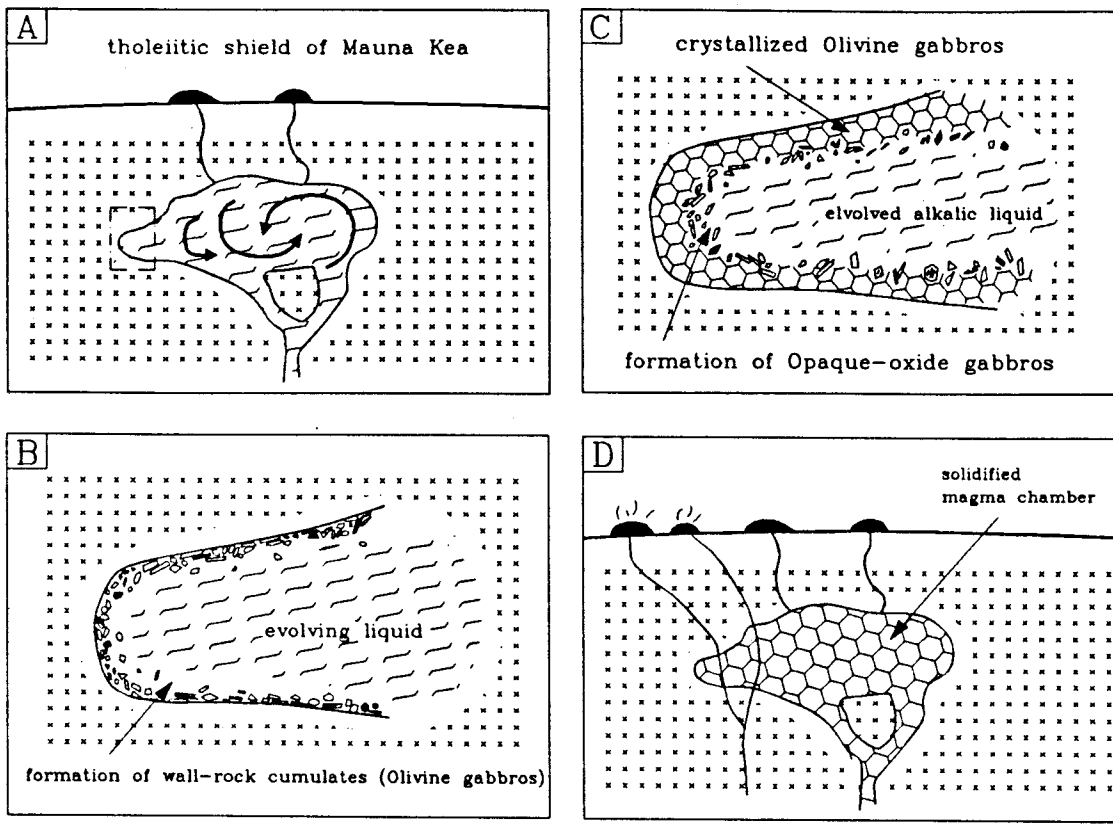

Fig. 9: Formation of olivine and opaque-oxide gabbros during the post-shield stage of Mauna Kea (after Fodor and Vandermeyden, 1988): a.) basaltic magma is cooling slowly in a shallow level magma chamber b.) an enlargement of a section from a.: olivine gabbros form in a boundary layer along the wall of the magma chamber; parts of the evolving liquid might erupt as Hamakua lavas c.) extensive crystallization in the advancing boundary layer results in formation of opaque-oxide gabbros d.) hawaiitic magma from a deeper source incorporates the gabbros of the solidified magma chamber during ascent to the surface.

composition ascended from a lower source, incorporated the xenoliths and took them up to the surface.

Another group of authors suggests a different course for the post-shield history at Mauna Kea (Fig. 10): Large volumes of magma produced during the shield-building stage, led to the formation of a shallow magma chamber in the upper crust. Frey et al. (1990) claimed that the diminishing eruption rate towards the end of the shield-building and during the post-shield stage was caused by a decrease in melt production in the mantle. Sr, Nd and Pb isotopic constraints imply a compositionally homogeneous source that produced tholeiitic and alkalic lavas by variable degrees of melting (Kennedy et al., in prep.). Slowly cooling magma chambers at shallow crustal levels underwent extensive fractionation, hence providing ideal conditions for the formation of high Fe-Ti-basalts. The fractionated liquid eventually erupted as the Hamakua Volcanics and left a gabbroic assemblage behind, that resembled the ol-gabbroic xenoliths. Decreasing magma-supply prevented fresh basaltic magma from ascending through the crust. Therefore, the magma accumulated at a lower level, perhaps at the crust-mantle boundary. Sufficient density differences between wall-rock and liquid after fractionation resulted in the eruption of Laupahoehoe Volcanics at the surface (Frey et al., 1990). This statement can be supported by the fact that Laupahoehoe Volcanics are nearly aphyric and free of phenocrystic clinopyroxene (West et al., 1988). Laupahoehoe geochemistry, however, indicates a need for clinopyroxene crystallization, a phenomenon that can be explained by moderate-pressure fractionation at greater depths when clinopyroxene replaced olivine as the liquidus phase (Mahood & Baker, 1986).

Figure 11 shows a schematic diagram of Sr/Zr versus Zr. The two trends reflect a decrease in Sr abundance due to the fact that plagioclase is a major fractionation phase for both the Hamakua and the Laupahoehoe lavas. Similar Sr/Zr starting compositions for both trends indicate their common parental source. Hamakua Volcanics formed from a Zr-poor parent at lower pressure.

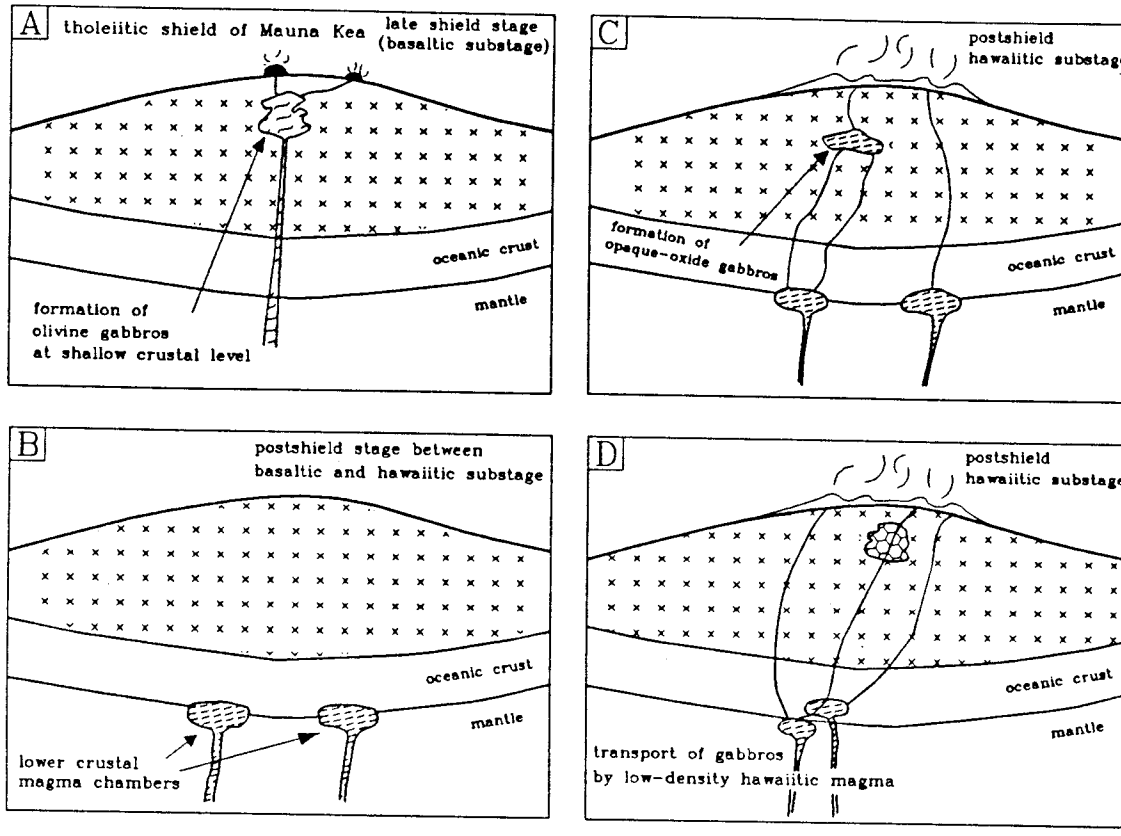

Fig. 10: Post-shield events at Mauna Kea (after Frey et al., 1990): a.) during late post-shield stage, basaltic liquid is slowly cooling in a shallow magma-chamber; fractionation results in segregation of olivine gabbros and eruption of residual Hamakua lavas b.) decreasing magma supply seizes ascent into upper crust; basaltic magma ponds in chambers at crust/mantle boundary c.) moderate-p crystallization produces a parental liquid that eventually segregates clinopyroxene-rich opaque-oxide gabbros; perhaps eruption of some evolved liquid d.) after extensive crystallization, low-density hawaiitic magma carries the gabbros up to the surface.

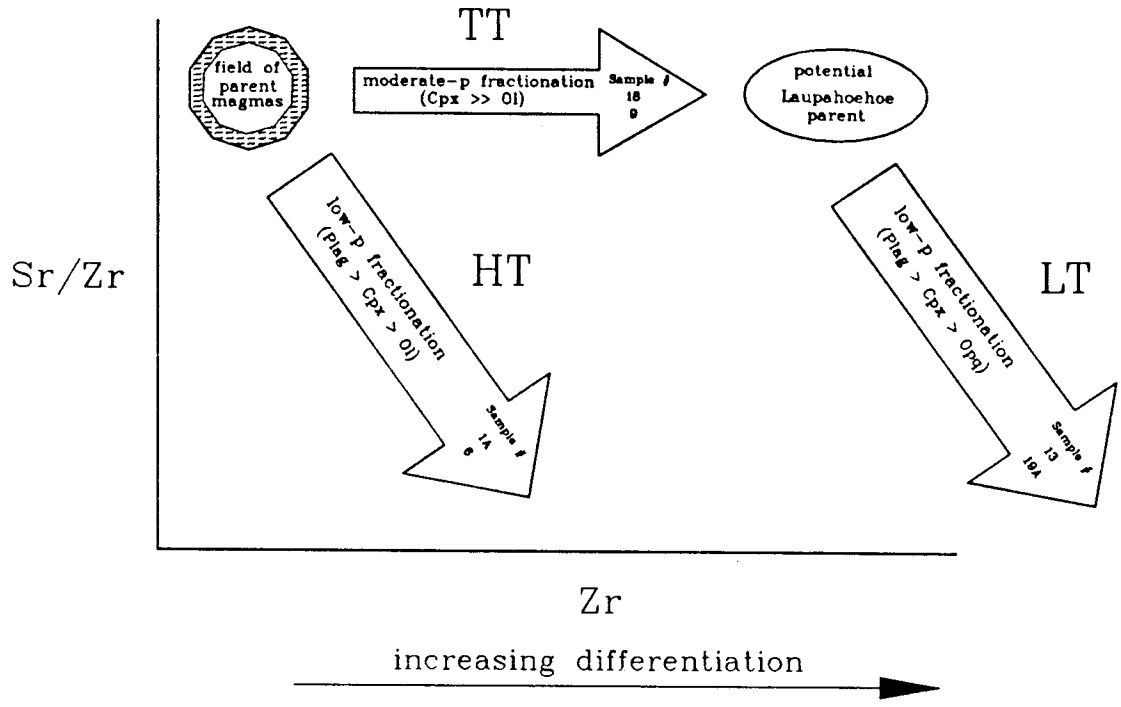

Fig. 11: Sr/Zr versus Zr for Mauna Kea post-shield lavas. Both trends (HT & LT) reflect Sr depletion in the melt by fractionation of plagioclase. Different degrees of melting of a common source (polygon) produce starting compositions for low-p fractionation of olivine gabbros and for an intermediate moderate-p fractionation that yields an incompatible element richer potential Laupahoehoe parent (ellipse). The sample numbers indicate gabbroic xenolith proto-examples for the three fractionation trends. The fractionating mineral assemblage is listed in parenthesis. (after Frey et al., 1990)

A different degree of melting yields a magma that segregated a clinopyroxene-rich assemblage under moderate-pressure conditions (TT).

The residual liquid with a higher amount of Zr, indicating the increase in differentiation, eventually is a potential parent magma that fractionates at lower pressure to form Laupahoehoe Volcanics. I have used this scheme to subdivide Fodor and Vandermeydens two gabbroic groups: the olivine gabbros can be split in a Hamakua trend (HT) with modal plag > cpx > ol, and a Transitional Trend (TT) for the moderate pressure assemblage with modal cpq > ol = plag while the opaque-oxide gabbros are related to Laupahoehoe volcanism by modal plag > cpx. Modelling of fractionation within the Laupahoehoe lavas by West et al. (1988) also showed that the composition of these lavas can be attained by a clinopyroxene-rich, plagioclase-poor, olivine and Fe-Ti-oxide bearing assemblage, agreeing closely with the opaque-oxide gabbros of Fodor and Vandermeyden. But despite detailed geochemical studies and intensive modelling, Frey and his coworkers (1990) do not exclude the possibility that Laupahoehoe lavas might have fractionated from a Hamakua parent, which would in fact be compatible with the proposal of Fodor and Vandermeyden (1988).

Chapter 4

4. Application of the model / Results

A proper application of the model is only feasible when a.) trace elements, each exhibiting a specific compatibility behaviour, enable one to deduce a sequence of crystallization, b.) a suite of volcanic rocks shows trace element features that distinguish these rocks as the complementary liquid trend to the segregated cumulates, and c.) the trapped liquid component in the cumulate pile is *not* host lava that carried the xenoliths up to the surface. Looking at the latter was one of the aims in doing this study: electron microprobe analyses of trace elements in the trapped liquid phase of Mauna Kea gabbroic xenoliths were performed to allow a comparison between the calculated information from the model - especially the composition of trapped liquid - and Fodor and Vandermeyden's data and interpretation of the liquid component (Fodor and Vandermeyden, 1988). A detailed discussion about this topic will be presented in a later section .

4.1. Selection of trace elements

As mentioned in earlier chapters, four trace elements were selected to test the model. Cr, Zr, Ni and Sr were chosen because of their higher abundances relative to the other trace elements in the whole-rock xenoliths and because of the distinctive nature of their individual partitioning behaviour. Transitional elements like Cr and Ni are especially useful because of their early partitioning into first-formed ferromagnesian minerals. Although it is a somewhat paradoxical relationship with respect to Mg-partitioning, Ni has a strong preference for the tetrahedral sites of olivine (Burns, 1973). Cr is taken up into the octahedral sites of clinopyroxene and is also a major constituent of spinel. Both

elements show - dependent on the sequence of minerals crystallizing out of the liquid - a decrease in relative abundance during the fractionation course of a melt and are therefore highly qualified for the establishment of a differentiation trend in a suite of rocks.

Sr is almost exclusively partitioned into plagioclase among the major silicate minerals and is taken up rather by the sodic than by the calcic member of the plagioclase crystallization-series (Korringa et al., 1971). All three elements Cr, Ni and Sr exhibit a more or less compatible behaviour since they are concentrated in appropriate minerals. In contrast, Zr is a valuable indicator for the advanced degree of fractionation due to its accumulation in the melt, in the absence of zircon saturation.

Commonly, the partition coefficient is defined as the ratio of the concentration of an element in the mineral versus the concentration of an element in the liquid with which it is in equilibrium. The bulk partition coefficient is a function of all phases crystallizing from the liquid whereby the dominant phase that displays the highest mineral/liquid partition coefficient determines the size of the bulk coefficient.

As much as the partitioning behaviour of the trace elements is one of the "supporting pillars" of this model, it also bears a large factor of instability: the exact partition coefficients between minerals and liquid are, despite experiments and direct measurements, only an approximation to the real situation, mainly due to the lack of constancy during the process of crystallization. Several different parameters were found to have an influence on the change of this coefficient during crystallization. Chromium distribution is dependent on the oxygen fugacity f_{O2} of the melt, resulting in either the formation of Cr^{3+} or Cr^{2+} (Barnes, 1986). The model itself does not specifically take into account the valence state of an element. However, both states show a different partitioning behaviour with Cr^{3+} having a priority in formation under terrestrial conditions (Huebner et al., 1976). The partition coefficient for Ni is strongly affected by T and melt-composition (Kinzler et al.,1990; Leeman & Lindstrom, 1978) which is

actually due to a mutual dependence of these parameters during fractionation (Hart & Davis, 1978). Drake and Weill, (1975), reported a T-dependence for Sr concentration in plagioclase. Changes in melt-composition as well as in T are responsible for the behaviour of Zr in the late melt (Watson & Harrison, 1984).

All of the above authors assumed equilibrium conditions for their studies, as generally no deviation of Henry's Law was observed. Unfortunately, the complexity of element distribution between mineral and liquid cannot be covered by a *constant* partition coefficient during the whole span of a cooling process. Nevertheless, it has to be pointed out that it does not seem to be justified to accommodate the distribution coefficients to every single step of the fractionation procedure. However, an attempt was made to distinguish three, petrographically different fractionation trends (TT, HT & LT, see chapter 3) and associate them with three different sets of partition coefficients. For these three sets (table II) that are partly adopted from the literature and partly own estimates for a better fitting of the petrographic data, comparable values of the literature are given in table III.

4.2. Application process

Originally, this trace element model was conceived for only two elements (DeLong & Chatelain, 1989). For the extended version with four elements, a simple approach was used to constrain the fixed parameters, like partition coefficients and starting compositions, by forming compatible-incompatible trace element pairs like Cr-Zr, Ni-Zr and Sr-Zr. With these single pairs, calculations were performed using the initial version of the model for two elements with optimized starting compositions and partition coefficients. These values were then modified for the calculations with all four elements in the extended model.

TABLE II Partition coefficients used for the model - data from Irving and Frey, 1984, Kinzler et al. 1990, and own estimates

		Dcpx/l	Dol/l	Dpl/l	Dspl/l	Dopq/l	Dap/l
Cr	TT*	13	1.1	0.02	2	10	0.01
	HT**	13	1.1	0.02	2	10	0.01
	LT***	13	1.1	0.02	2	10	0.01
Zr	TT	0.07	0.01	0.01	0.1	0.02	0.01
	HT	0.15	0.01	0.01	0.1	0.02	0.01
	LT	0.15	0.01	0.01	0.1	0.02	0.01
Ni	TT	8	6	0.06	4	1.5	0.2
	HT	8	7.5	0.06	4	1.5	0.2
	LT	6	15	0.06	4	1.5	0.2
Sr	TT	0.08	0.014	0.58	0.01	0.01	2
	HT	0.1	0.014	1.65	0.01	0.01	2
	LT	0.11	0.014	1.35	0.01	0.01	2

* TT = Transitional Trend
** HT = Hamakua Trend
***LT = Laupahoehoe Trend

TABLE III Comparable partition coefficients from the literature

	Dcpx/l	Dol/l	Dpl/l	Dspl/l	Dopq/l	Dap/l
Cr	12 - 15.5 Irving & Frey 1984	3 Irving 1987	-	-	6 Irving 1978	0.048 Irving & Frey 1984
Zr	0.12 Irving 1978	0.01 Pearce & Norry 1979	0.01 Irving 1978	-	0.02 Pearce & Norry 1979	-
Ni	8 - 10 Lindstrom & Weill 1978	14 - 19 Leeman & Lindstrom 1978	0.04 Lindstrom 1976	5.9 Irving 1978	12.2 - 19.4 Leeman 1974	0.43 Irving & Frey 1984
Sr	0.08 - 0.11 Hart & Brooks 1974 0.15 Sun et al. 1974	0.09 Philpotts & Schnetzler 1970	1.5 - 2.3 Irving 1978	-	-	2.7 Irving & Frey 1984

Taking Cr and Zr as a general example of a compatible-incompatible pair, the following discussion demonstrates how these fixed parameters were obtained. As a prerequisite for the model, the erupted rocks at Mauna Kea - the Hamakua and the Laupahoehoe Volcanics - are assumed to define one or more liquid line(s) of descent (LLD) from which the gabbroic rocks formed in equilibrium. Geochemical data by Frey and coworkers (1990) for the Hamakua lavas as well as studies of Laupahoehoe lavas by West and coworkers (1988) were taken to fit a fractionation curve (LLD) based on the Rayleigh Fractionation Law (Eq. 8) through the respective trace element data. The data are displayed in two separate diagrams: Figure 12 exhibits the trace element concentrations for the Hamakua Volcanics and the respectively calculated Hamakua and Transitional complementary liquid lines of descent (HT & TT). Figure 13 shows the same configuration for the opaque-oxide gabbros and their related Laupahoehoe liquid trend (LT). The convention for each of the diagrams is kept during the course of this study. To calculate the principal features of the fractionation process - the proportions of the precipitated minerals, the remaining part of the original liquid, and the composition and proportion of the trapped liquid component, it is especially important to select a reasonable starting composition for these fractionation trend.

4.3. Starting compositions and partition coefficients

Frey and coworkers (1989) studied the transitional events between the eruptions of Hamakua and Laupahoehoe Volcanics by least square modelling of major elements. They chose their ankaramitic samples #115-12 and #97-14 as possible parents for the Laupahoehoe lavas.

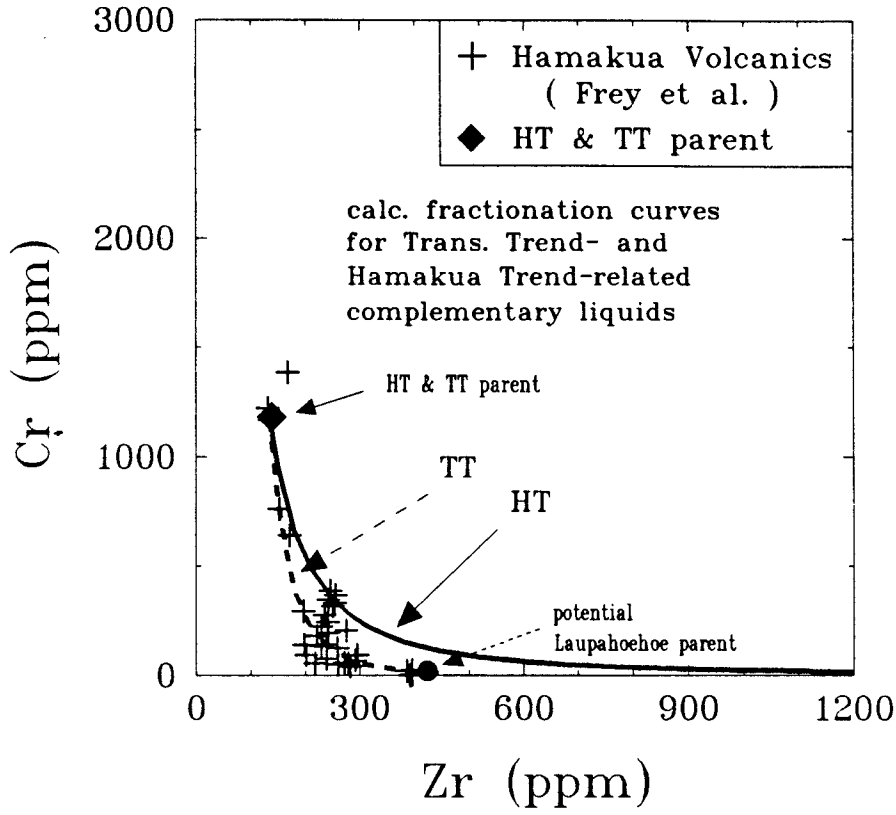

Fig. 12 : Cr against Zr for the olivine gabbros (general trends). Crosses = Hamakua Lavas, (Frey et al., 1990), filled diamond = parental composition, solid line = Hamakua Trend, dashed line = Transitional Trend. The key is utilized for all other olivine gabbro diagrams.

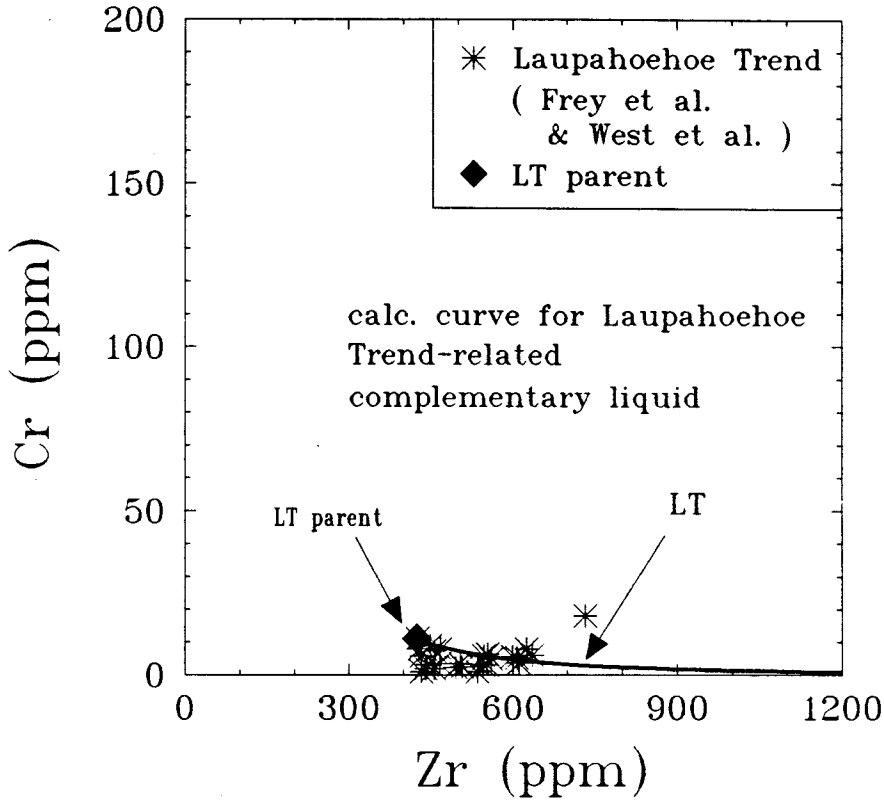

Fig. 13 : Cr against Zr for opaque-oxide gabbros (general trends). Note different scale. Stars = Laupahoehoe lavas (Frey et al., 1990, and West et al., 1988), filled diamond = parental composition, solid line = Laupahoehoe Trend. This key is utilized for all other opaque-oxide diagrams.

Care had to be taken not to pick a sample that showed accumulated features like MgO-enrichment or $Al_2O_3/CaO < 0.9$, a criterion for clinopyroxene accumulation. Both samples appear to have the least evolved trace element geochemistry and are able to yield a hawaiitic composition by segregation of a gabbroic assemblage that resembles Fodor and Vandermeyden's olivine gabbroic xenoliths. Thus, I adopted sample #115-12 from Frey and coworkers as a parental composition for all Hamakua and Transitional Trend trace element pairs.

As shown in Figure 11, Laupahoehoe lavas have a more evolved initial composition than Hamakua lavas. Magma that probably originated by different degrees of melting from the same source as the Hamakua Volcanics underwent an intermediate state of moderate-pressure crystallization (TT), providing a residual liquid composition close to the Laupahoehoe parent. In the case of the fractionation curve for the Transitional Trend, a line was fitted through the data of Frey and coworkers that aims towards a potential Laupahoehoe parent (Fig. 12). This parent was specified by West and coworkers, (1988), who took their sample #Mi-5, that is the most mafic Laupahoehoe hawaiite, for major element least squares modelling. The trends for the single trace element couples were individually calculated by taking the "best-fit" source composition. The establishment of "best-fit" compositions is explained by the fact that the determination of the parent involves a factor of heterogeneity in the source and a "field" of parental compositions is petrologically more adequate to obtain a "best-fit" fractionation curve. Table IV shows the source compositions (which were taken for the extended four-element model) according to Frey and West and coworkers and the slightly different "best-fit" numbers for the single trace element pairs. The D*s (Dstars) were likewise selected to fit a theoretical Rayleigh fractionation curve through the data. Consequently, D_{Cr} and D_{Zr}, which are variables of D* (Eq. 32), can be found by assuming one number and calculating the other (Table V).

TABLE IV Starting compositions
after Frey et al., 1990, and West et al., 1988)

	Cr	Zr	Ni	Zr	Sr	Zr
HT*	1167	135	486	135	380	135
("Best-Fit" HT)	-	-	(490	131)	-	-
TT**	1167	135	486	135	380	135
("Best-Fit" TT)	-	-	(490	131)	-	-
LT***	10.8	425	13	425	1260	425
("Best-Fit" LT)	-	-	(13	428)	(1310	425)

* Hamakua Trend
** Transitional Trend
*** Laupahoehoe Trend

TABLE V Dstar and bulk partition coefficients

	TT	HT	LT
D*	-3.8	-1.95	-2.4
Dzr	0.02	0.02	0.02
Dcr	4.72	2.92	3.35
		Best-Fit	
D*N	-3	-1.8	-1.3
Dzr	0.01	0.02	0.01
Dni	3.97	2.76	2.29
D*S	0.92	0.55	-0.36
Dzr	0.03	0.02	0.03
Dsr	0.09	0.46	0.63

TT = Transitional Trend
HT = Hamakua Trend
LT = Laupahoehoe Trend

One might ask, why D^* in the final part of the mathematical derivations (Eq. 34 - 36) is a function of D_{Cr} and D_{Zr} and not of D_{Sr} or D_{Ni} and D_{Zr}. The behaviour of Sr is somewhat enigmatic and is considered in detail in a later part. Unlike Cr, Ni-distribution, as previously discussed, is much more dependent on changes during cooling than Cr. However, for the calculations it is of fundamental importance to pick the one trace element pair that suggests the scientifically most reliable and predictable course of fractionation. This pair, here Cr and Zr, act as key variables in the iterative part of Eq. 32 (see chapter II). Hence, the concentrations of all elements in the trapped liquid are based on the Cr - Zr relationship.

Figures 12 to 17 depict the calculated LLDs for the different compatible-incompatible trace element pairs that were used in the extended model. Figure 17 shows an example for the displacement of the "Best-Fit" trend for the single-pair model from the calculated liquid trend with West and coworker's (1988) starting value. After these introductory figures, the computational results for the extended model are presented, each in comparison with the calculated single-pair model output. The way all calculated results are depicted is essentially according to Figure 1, where the relationships of a compatible and an incompatible trace element during a differentiation process are displayed for the whole-rock gabbroic xenoliths, the fractionating liquid (=the presumably complementary suite of volcanic rocks) and a mixture of both phases which is reflected by the trapped liquid composition (=calculated results C^l_ξ) in the gabbro. Additionally, the petrological separate trapped liquid phase of three xenolith samples was analysed on the electron microprobe for a variety of major and trace elements (Table VI).

These analyses are one of the most relevant parameters for the accomplishment of this study. Calculated results and eventually the mathematical proceedings of the model itself are tested against "real" values (=trace elements concentrations) of the glass component in the gabbroic xenolith.

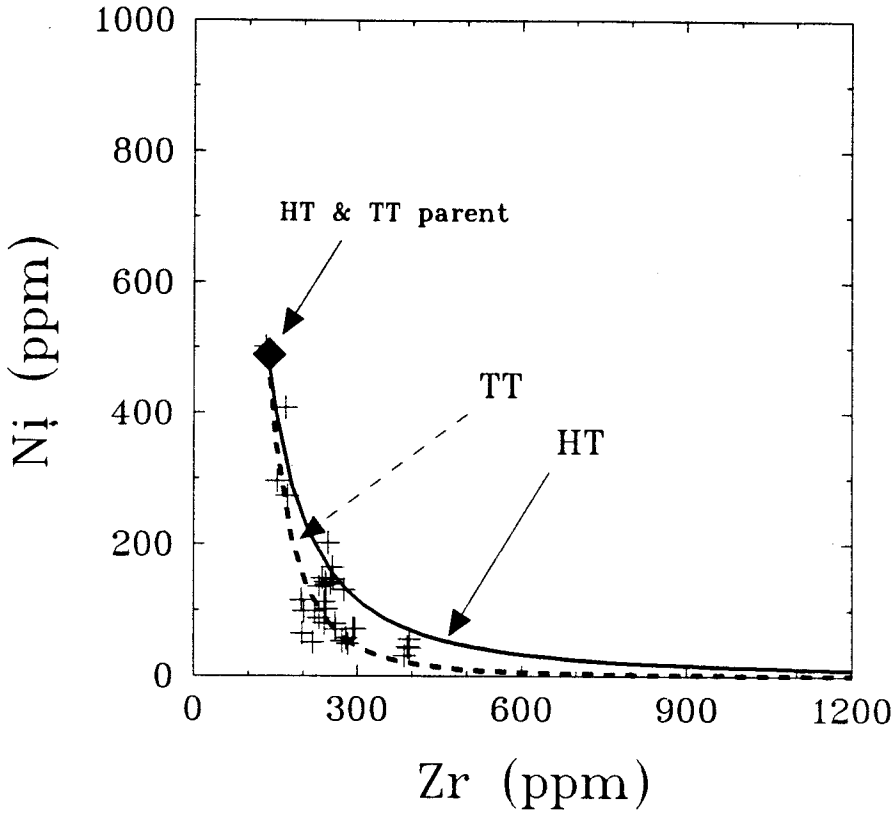

Fig. 14 : Ni against Zr for olivine gabbros (general trends).
For key see Fig. 12.

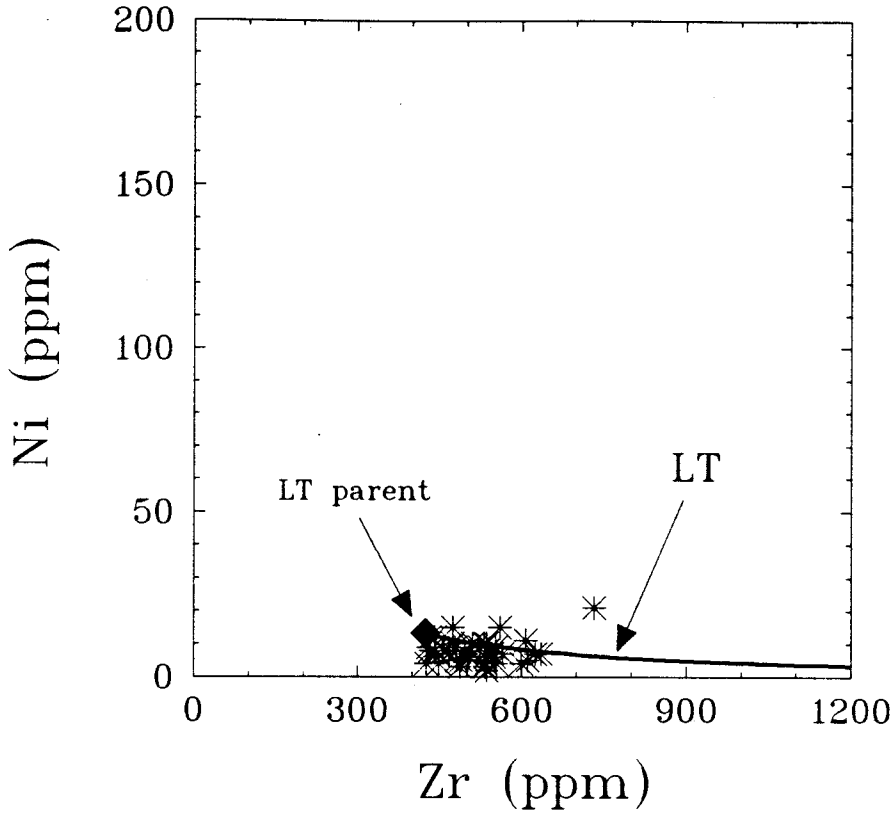

Fig. 15 : Ni against Zr for opaque-oxide gabbros (general trends). Note different scale. For Key see Fig. 13.

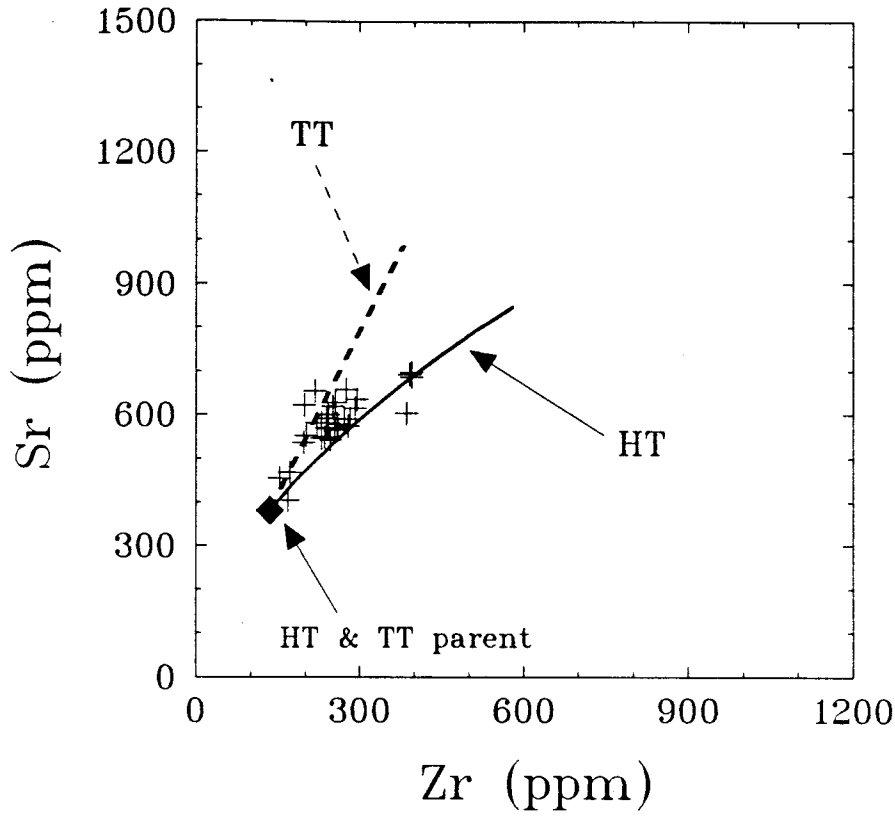

Fig. 16 : Sr against Zr for olivine gabbros (general trends). Positive trends are due to $0 < D^* < 1$.
For key see Fig. 12.

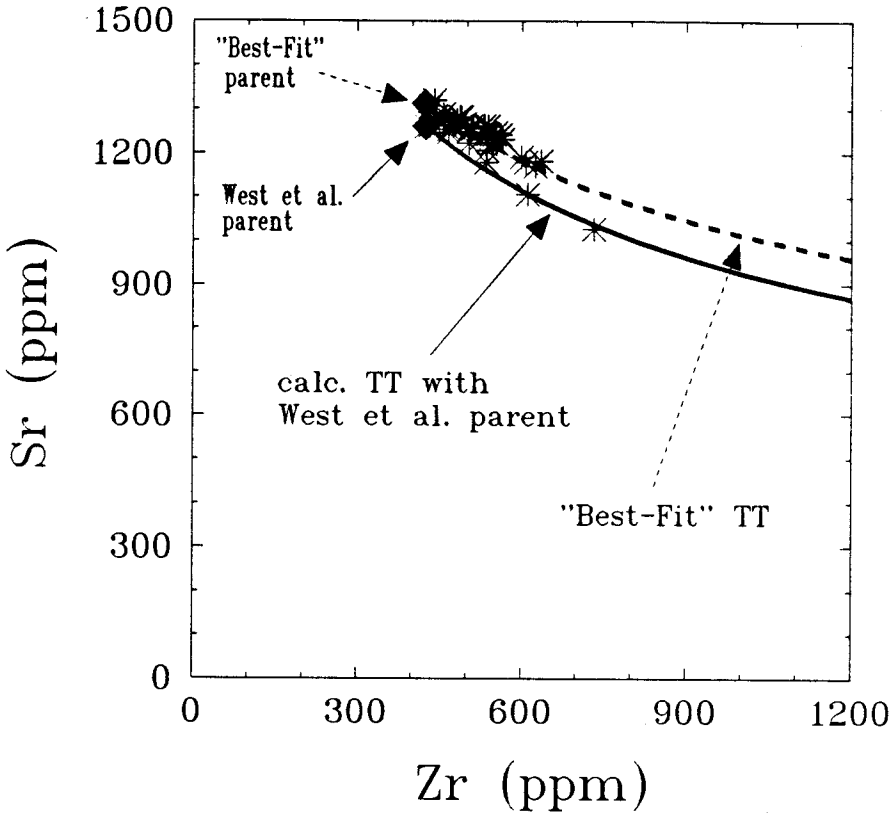

Fig. 17 : Sr against Zr for opaque-oxide gabbros (general trends). The calculated trend starting with West and coworker's value (1988) is compared with the "Best-Fit" trend for the single-pair model. For key see Fig. 13.

TABLE VI Comparison of Fodor and Vandermeyden's (FV) glass analyses (1988) with duplicate analyses of this study (U) (major elements in wt. %, trace elements in ppm)

	Olivine Gabbros		Opaque-oxide Gabbros			
sample#	9-FV	9-U	13-FV	13-U	19A-FV	19A-U
SiO2	54.40	50.06	51.60	51.47	51.00	50.06
TiO2	3.00	3.13	3.40	3.37	3.00	3.34
Al2O3	16.70	15.73	15.30	15.35	14.70	14.51
FeO*	7.10	7.83	10.20	9.64	12.40	11.78
MnO	0.13	0.19	0.18	0.19	0.15	0.26
MgO	2.80	2.59	3.20	3.09	3.60	3.47
CaO	5.00	5.33	6.30	6.70	7.60	7.55
Na2O	4.60	5.98	4.60	5.78	4.10	4.89
K2O	4.00	4.12	2.80	2.98	2.80	2.67
P2O5	1.00	0.98	1.40	1.15	1.30	1.48
Total	98.73	98.04	98.98	99.73	100.65	100
Zr	-	955	-	854	-	807
Cr	-	44	-	19	-	15
Ni	-	62	-	22	-	14
Sr*	300	708	400	957	400	1002
Ba*	800	-	1000	-	700	-

* reported as SrO and BaO by Fodor and Vandermeyden (1988)

During further discussion of the compatible-incompatible trace element diagrams, an attempt was made to evaluate the scientific "reality" of the microprobe glass analyses and hence whether the glass in the xenoliths is 'true' trapped liquid or merely host rock that was injected into the gabbros during ascent to the surface.

4.4 Analytical techniques for the microprobe data

Trace-element concentrations in the glass phases of three samples (#9, #13, #19A) were determined with a JEOL electron-microprobe by Dave Wark at Rensselaer Polytechnical Institute (RPI). Analytical conditions were 15 kV accelerating potential, a counting time of 96 min and a beam-current of 100nA with a beam-diameter of 25 μm. Most analyses were within 2 σ standard deviation of the nominal values. Detection limits (2 σ) are 14 ppm for Cr, V and Zr, 12 ppm for Sr and 23 ppm for Ni. Analytical errors are below $\approx$ 12 % for Cr and Sr, below $\approx$ 20 % for Zr and below $\approx$ 40 % for Ni. The accuracy of secondary standard analyses is given in Fig. 23, showing a moderate (Sr) to good (others) reproductibility for the trace elements. Major elements were analyzed with an accelerating potential of 15kV, a counting time of 20 s and a beam current of 15 nA. The Bence-Albee procedure was used to perform appropriate matrix corrections for the major elements (Bence and Albee, 1968).

4.5. Results

Table VII and Table VIII show the calculated results for the extended version and the single-pair model, respectively.

By looking at the Hamakua Trend and Transitional Trend diagrams for Cr and Ni (Fig. 18, 19, & 20), the gabbros evidently join a line that is quite comparable to the LLDs, but with a lower Zr-content at a given Cr-concentration in the sample. This implies that both diagrams for Cr and Ni are relatively consistent with the simple mixing state of Figure 1.

TABLE VII Computer-calculated results of the extended version of the model

(Zrl, Crl, Nil and Srl in ppm)

sample#	F	Zrl	Crl	Nil	Srl	Xliq	Xplag	Xcpx	Xsl	Xol	Xap	Xopq	Nio	Sro
Olivine Gabbros														
Trans. Trend														
2A	0.7	191	313	175	570	0.14	0.18	0.38	0.001	0.3	0	0	62	783
2B	0.7	191	310	174	668	0.15	0.21	0.38	0	0.26	0	0	61	921
9	0.72	186	345	145	451	0.3	0.12	0.41	0.006	0.18	0	0	55	606
4	0.76	177	417	136	615	0.33	0.14	0.34	0.008	0.17	0	0	60	789
18	0.74	181	381	114	348	0.26	0.05	0.54	0	0.16	0	0	47	457
1B	0.72	185	351	138	501	0.31	0.13	0.38	0.03	0.15	0	0	54	671
8	0.7	192	308	127	728	0.28	0.2	0.4	0	0.12	0	0	44	1005
Hamakua Trend														
6	0.53	251	347	146	673	0.3	0.28	0.23	0	0.2	0	0	50	948
3A	0.36	369	164	59	702	0.15	0.31	0.45	0.005	0.09	0	0	10	1219
1A	0.38	352	180	102	660	0.21	0.36	0.35	0.002	0.07	0	0	18	1118
3B	0.25	531	81	82	668	0.11	0.41	0.43	0	0.06	0	0	7	1415
11	0.33	405	137	82	841	0.16	0.31	0.46	0	0.07	0	0	11	1539
Opaque-Oxide Gabbros														
14	0.43	978	1.5	2.5	612	0.03	0.11	0.52	0	0	0	0.35	0.8	826
17A	0.44	959	1.5	5.6	961	0.09	0.36	0.3	0	0	0	0.25	2	1287
12	0.44	956	1.5	5.1	925	0.09	0.36	0.31	0	0.001	0	0.24	1.8	1238
15B	0.43	962	1.5	4.3	948	0.08	0.36	0.31	0	0	0	0.25	1.5	1272
13	0.42	987	1.4	23	908	0.11	0.33	0.41	0	0	0	0.16	7.5	1230
16	0.44	955	1.5	3.7	1265	0.12	0.33	0.27	0	0	0	0.29	1.3	1695
19A	0.5	836	2.1	7	929	0.16	0.37	0.21	0	0	0.08	0.19	2.9	1185

TABLE VIII Computer-calculated results for the single-pair model

			Cr against Zr			(Zrl, Crl, Nil and Srl in ppm)				
sample#	F	Zrl	Crl	Xliq	Xplag	Xcpx	Xsl	Xol	Xap	Xopq
Olivine Gabbros										
Trans. Trend										
2A	0.7	191	309	0.13	0.18	0.39	0	0.3	0	0
2B	0.7	192	306	0.14	0.21	0.39	0	0.26	0	0
9	0.72	187	339	0.28	0.12	0.41	0.006	0.18	0	0
4	0.76	178	411	0.32	0.15	0.35	0.008	0.17	0	0
18	0.74	182	373	0.24	0.05	0.55	0	0.17	0	0
1B	0.72	186	345	0.29	0.14	0.39	0.03	0.15	0	0
8	0.7	193	303	0.27	0.21	0.4	0	0.12	0	0
Hamakua Trend										
6	0.54	249	353	0.31	0.27	0.22	0	0.19	0	0
3A	0.62	214	203	0.34	0.24	0.35	0.003	0.07	0	0
1A	0.38	348	184	0.23	0.35	0.34	0.02	0.07	0	0
3B	0.25	524	83	0.14	0.39	0.42	0	0.06	0	0
11	0.6	222	178	0.39	0.22	0.34	0	0.05	0	0
Opaque-Oxide Gabbros										
14	0.19	772	1.54	0.08	0.1	0.49	0	0	0	0.33
17A	0.44	952	1.58	0.11	0.35	0.29	0	0	0	0.24
12	0.44	949	1.6	0.11	0.35	0.3	0	0.001	0	0.23
15B	0.44	955	1.55	0.09	0.35	0.3	0	0	0	0.24
13	0.43	978	1.46	0.13	0.32	0.39	0	0	0	0.16
16	0.44	949	1.57	0.13	0.32	0.26	0	0	0	0.28
19A	0.5	832	2.15	0.18	0.36	0.2	0	0	0.08	0.18

TABLE VIII (continued)

Ni against Zr

sample#	F	Zrl	Nil	Xliq	Xplag	Xcpx	Xsl	Xol	Xap	Xopq
Olivine Gabbros										
Trans. Trend										
2A	0.7	190	175	0.14	0.18	0.38	0.001	0.3	0	0
2B	0.7	191	174	0.15	0.21	0.38	0	0.26	0	0
9	0.65	205	140	0.26	0.12	0.42	0.006	0.19	0	0
4	0.63	212	127	0.27	0.16	0.37	0.009	0.19	0	0
18	0.6	225	107	0.2	0.05	0.58	0	0.18	0	0
1B	0.64	209	133	0.27	0.14	0.41	0.03	0.15	0	0
8	0.62	214	123	0.25	0.21	0.41	0	0.13	0	0
Hamakua Trend										
6	0.5	267	143	0.28	0.28	0.24	0	0.2	0	0
3A	0.29	449	56	0.11	0.33	0.47	0.005	0.09	0	0
1A	0.42	318	105	0.24	0.35	0.34	0.002	0.07	0	0
3B	0.38	347	89	0.21	0.36	0.38	0	0.05	0	0
11	0.37	359	84	0.19	0.3	0.44	0	0.07	0	0
Opaque-Oxide Gabbros										
14	0.38	1098	3.8	0.04	0.38	0.32	0	0	0	0.26
17A	0.53	795	5.8	0.12	0.34	0.29	0	0	0	0.24
12	0.49	860	5.2	0.11	0.35	0.3	0	0.001	0	0.23
15B	0.42	997	4.2	0.08	0.36	0.31	0	0	0	0.25
13	0.36	1166	3.5	0.08	0.34	0.42	0	0	0	0.17
16	0.37	1130	3.6	0.09	0.34	0.27	0	0	0	0.3
19A	0.63	670	7.2	0.22	0.34	0.19	0	0	0.07	0.17

TABLE VIII (continued)

Sr against Zr										
sample#	F	Zrl	Srl	Xliq	Xplag	Xcpx	Xsl	Xol	Xap	Xopq
Olivine Gabbros										
Trans. Trend										
2A	0.47	236	635	0.11	0.19	0.4	0.001	0.31	0	0
2B	0.32	318	836	0.08	0.23	0.42	0	0.28	0	0
9	not calculated									
4	0.26	378	979	0.13	0.19	0.45	0.001	0.22	0	0
18	not calculated									
1B	0.72	173	476	0.33	0.13	0.37	0.03	0.14	0	0
8	0.22	418	1075	0.11	0.26	0.49	0	0.15	0	0
Hamakua Trend										
6	0.31	427	716	0.15	0.33	0.28	0	0.24	0	0
3A	0.31	423	712	0.12	0.32	0.46	0.005	0.09	0	0
1A	0.36	371	662	0.2	0.37	0.36	0.002	0.007	0	0
3B	0.36	362	654	0.2	0.36	0.38	0	0.05	0	0
11	0.21	619	878	0.07	0.34	0.51	0	0.08	0	0
Opaque-Oxide Gabbros										
14	not calculated									
17A	0.25	779	1033	0.13	0.34	0.29	0	0	0	0.24
12	0.22	837	1007	0.12	0.35	0.3	0	0.001	0	0.23
15B	0.24	795	1026	0.11	0.35	0.3	0	0	0	0.24
13	0.19	893	984	0.13	0.32	0.4	0	0	0	0.16
16	0.68	503	1209	0.28	0.27	0.22	0	0	0	0.24
19A	0.21	844	1004	0.16	0.37	0.21	0	0	0.08	0.19

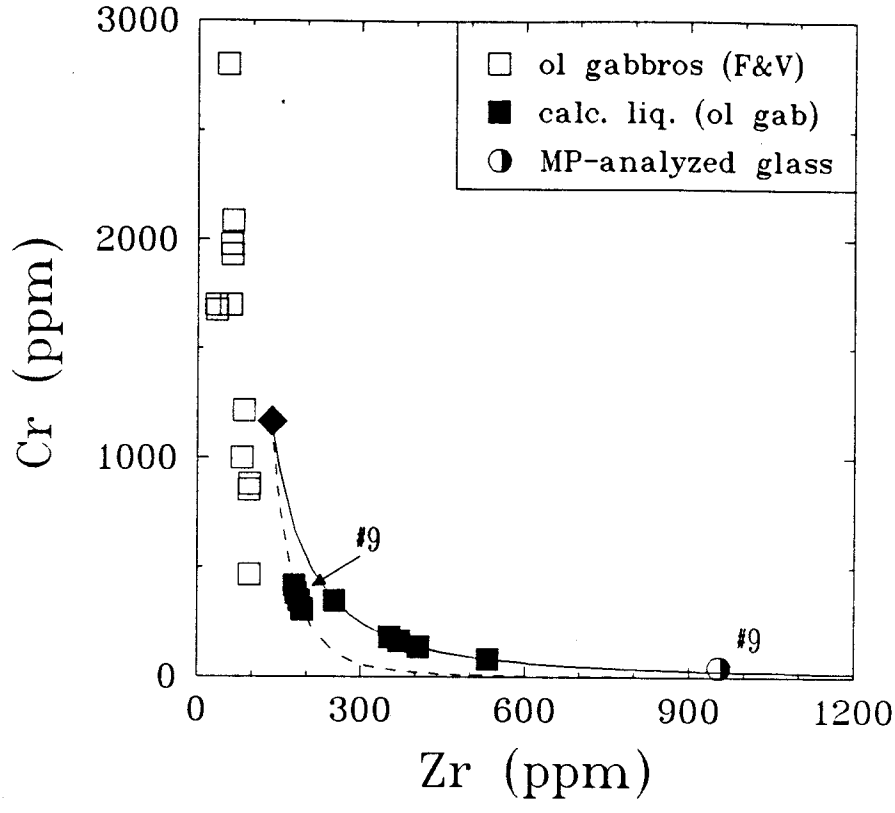

Fig. 18 : Cr against Zr for olivine gabbros. Filled squares represent the concentrations of the trace elements in the glass phase that were calculated with the model. Analyzed glass does not fall within a reasonable range of the calculated model-results. For analyt. error see section 4.4.

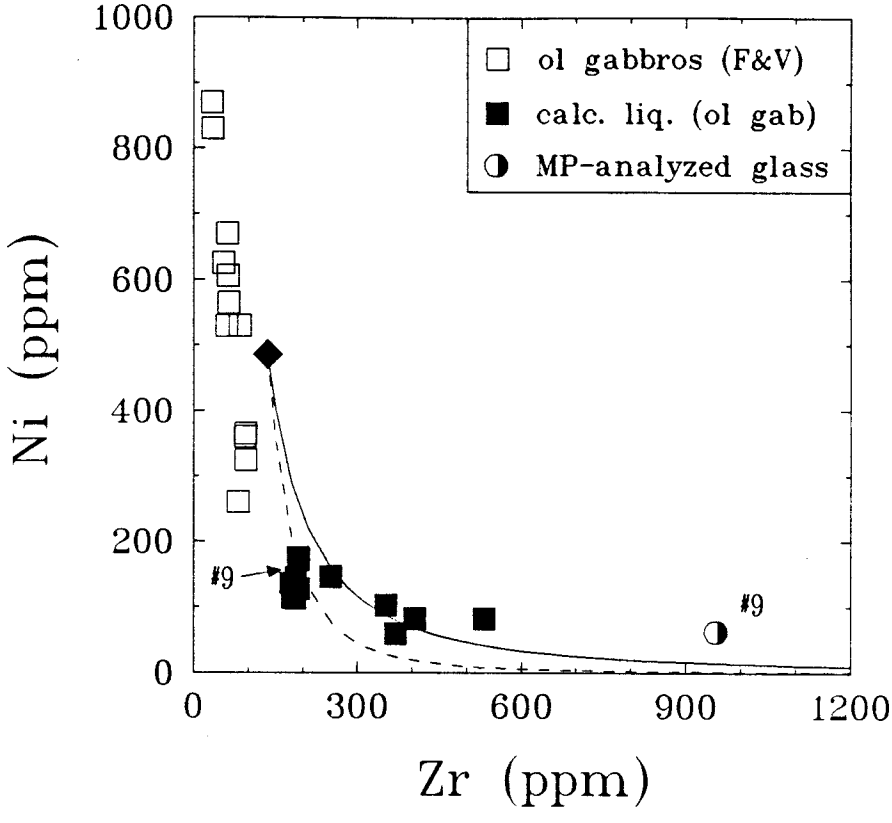

Fig. 19 : Ni against Zr for olivine gabbros (extended model). Note weak scatter. No agreement of calculated results and microprobe analyses. For analyt. error see section 4.4.

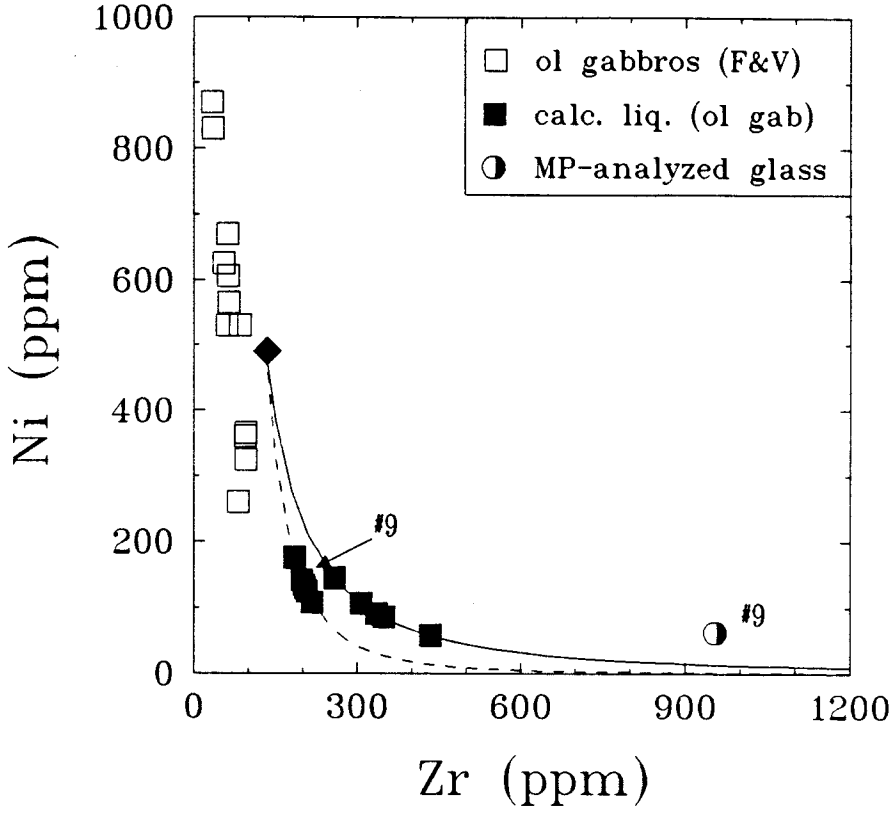

Fig. 20 : Ni against Zr for olivine gabbros (single-pair model). For analyt. error see section 4.4.

Comparing both types of results, from the extended and the single-pair model for the same pair of trace elements, it is obvious that for the single-pair model the calculated data fall nicely along the expected trends while for the extended version of the model, especially at the Sr - Zr diagrams, the computational output is scattered over a broader area (Fig. 21 & 22). As mentioned before, D* is solely a function of Dcr and Dzr in the single-pair model as well as in the extended model. In the single-pair type a single Rayleigh Fractionation curve is defined by one compatible-incompatible pair of trace elements. Although Cr and Zr play the major role in the extended model, there are actually four elements, exhibiting mutual dependence in their partitioning behaviour. Instead of establishing the Rayleigh curve with one single couple, three pairs of trace elements and therefore three different two-dimensional equations are associated with each other and form a multidimensional surface that would have to be projected on each compatible-incompatible diagram to obtain the ideal Rayleigh fractionation curve. Due to difficulties in mathematical representation this task was abandoned.

For the olivine gabbros, Cr is plotted against Zr in Fig. 18. The calculated concentrations for the trapped liquid component of both the medium and the lower pressure gabbros (TT & HT) occupy a reasonable position in this diagram to form a triangle with the solid phases, in which the mixture of all cumulate phases and the trapped liquid phase is located. Although one has to allow an error range for both the calculated samples and the microprobe analyses, it is obvious that the microprobe results for sample #9 display a much more advanced evolutionary state than all the computationally produced results. This statement is not only valid for the trace element data but also for the major elements. The glass in #9, an olivine gabbro, shows an even higher evolved major element composition than the glass in the opaque-oxide gabbros (Table VI), a fact not clearly recognized by Fodor and Vandermeyden (1988).

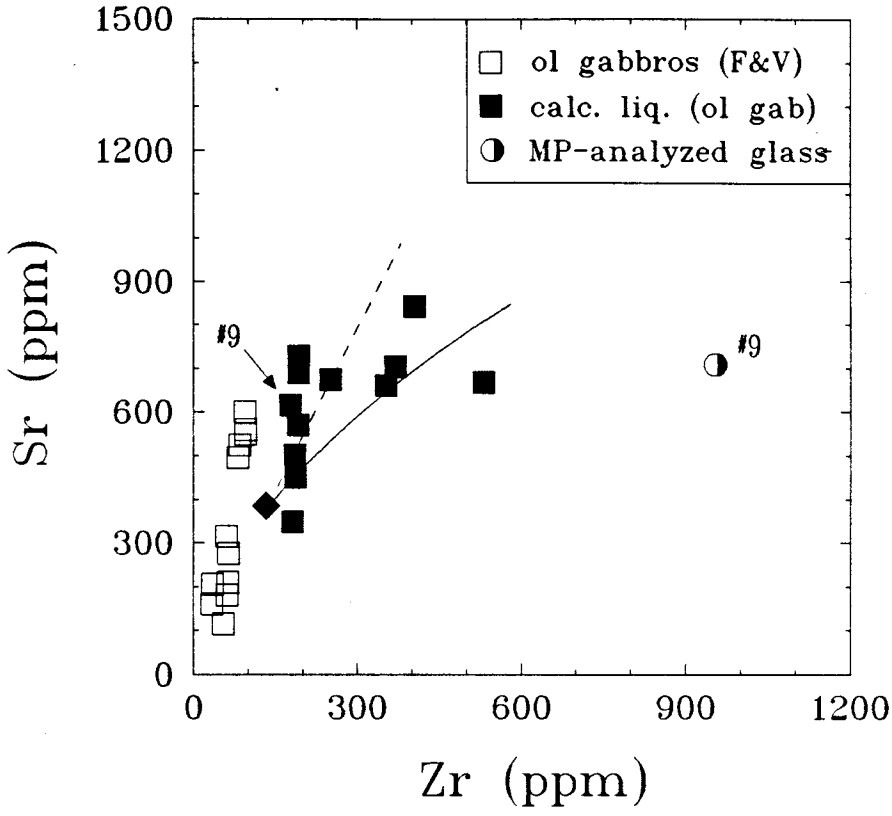

Fig. 21 : Sr against Zr for olivine gabbros (extended model). Remarkable scattering of calculated results, see text for further explanation. For analyt. error of MP-glass see section 4.4.

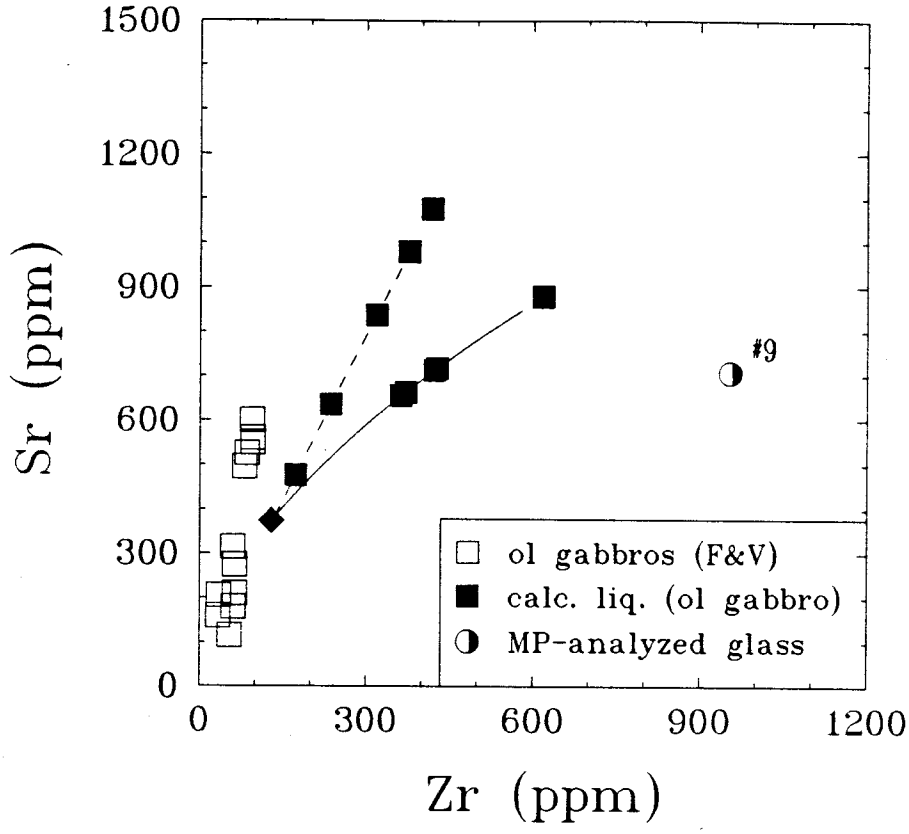

Fig. 22 : Sr against Zr for olivine gabbros (single-pair model). For analyt. error of the MP-glass see section 4.4.

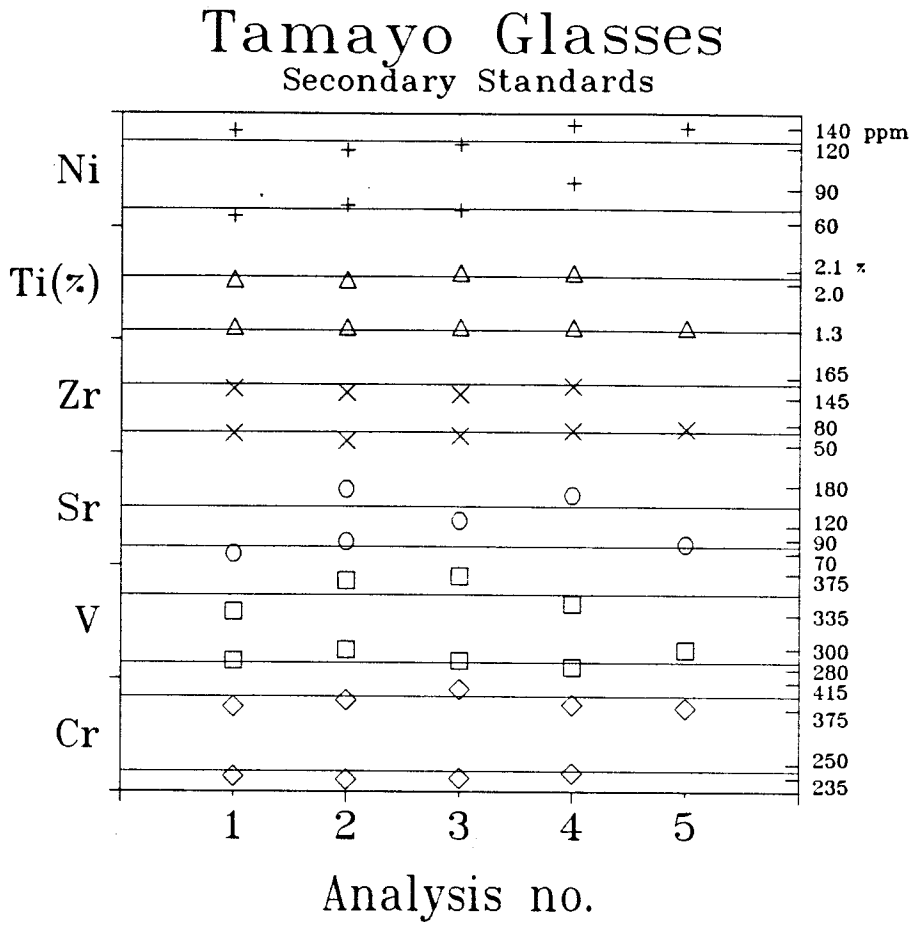

Fig. 23 : Secondary standards for trace element MP-analyses of the glass phase. Two different samples were analysed for the same element, each sample four times. The lines give the nominal values for the element concentrations while the numbers on the right ordinate represent values of the specific element.

Two possible reasons ought to be considered for an explanation: one, the mathematical algorithm might represent an approach too simple to cover the complexity of a cooling system. Also, starting composition and partition-coefficients can account for additional uncertainties.

The other possibility is that the interstititial glass has indeed the same composition as the hawaiitic host that penetrated the gabbros. Looking at the data of Frey and coworkers (1990, Table 1A), their Hamakua sample #5 has the highest Zr-content with 395 ppm. Even the most evolved sample of West and coworkers (1988, Table 1), Mi-4, a Laupahoehoe mugearite, does not exceed 636 ppm Zr. The $Mg^{\#}$ = 0.66 for the glass in gabbro sample #9 matches the general trend for either the Hamakua lavas (basalt sample #5 with $Mg^{\#}$ = 0.68), or the Laupahoehoe Volcanics (basalt sample #Mi-5 with $Mg^{\#}$ = 0.66). Thus, using a K_D = 0.3 (Roeder & Emslie 1970), the supposed trapped liquid phase is far too evolved to have been in equilibrium with olivine ($Fo^{\#}$ = 0.82) of olivine gabbro #9. Remelting of the gabbroic phases was excluded by Fodor and Vandermeyden, (1988), as the glass displays a homogeneous appearance in every sample. Additionally, zircon precipitation could not be detected. A plausible explanation for the composition of the glass might be given by further evolution of "trapped" host-hawaiite after penetration of the gabbros and during ascent to the surface.

For Ni and Zr a similar situation is observed in Fig. 19 & 20. Note the scattering of the data due to the simplified depiction of the partitioning behaviour among the different trace elements.

Opaque-oxide gabbros show an incompatible-compatible relationship, in general one order of magnitude lower than for the olivine gabbros. Laupahoehoe starting composition for Cr and Zr in Figure 24 might be a relic of moderate-pressure fractionation of a TT gabbroic assemblage at the crust-mantle boundary. Small inhomogeneities in melt composition give rise to dramatic changes in relative trace

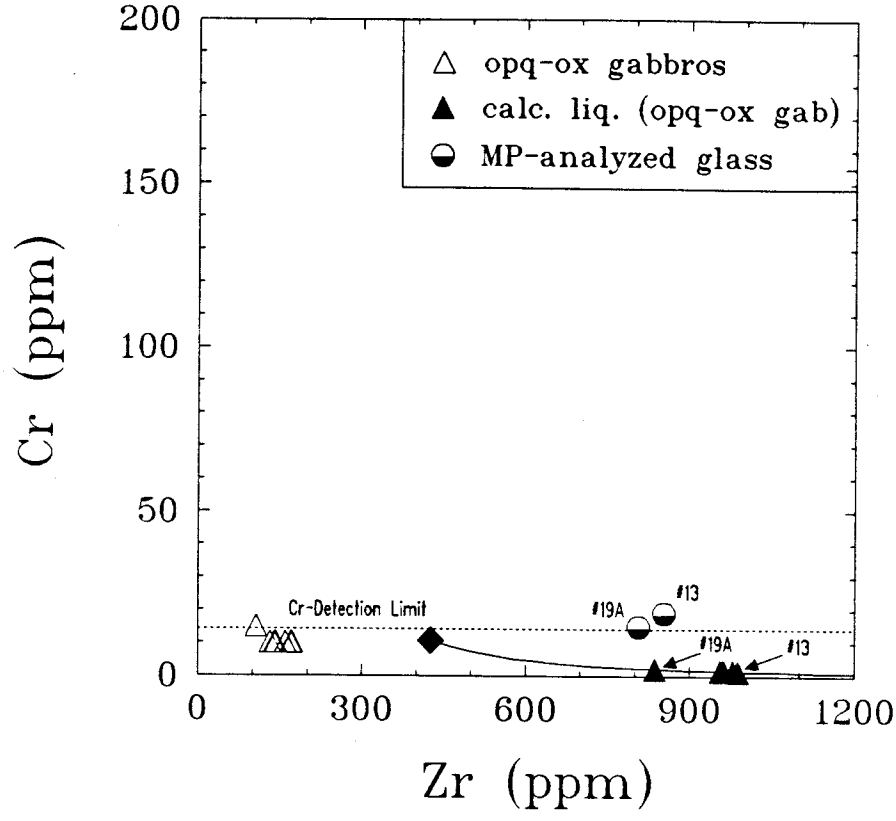

Fig. 24 : Cr against Zr for opaque-oxide gabbros (extended model). With a 2 sigma error = 2 ppm for Cr and 3 ppm for Zr, the MP-analyses might remain below the detection limit, thus the values merely give a qualitative statement for the liquid composition.

element abundances. Also, model parameters might be able to shift the calculated results in different directions.

Within analytical error, Cr and Ni are close to or remain under the detection limit for opaque-oxide gabbros. Despite these possible deviations (particularly high for Ni) the glass analyses for sample 13 and 19A are still located in a tolerable distance from the calculated data. At this point of the differentiation process, the LLD is not anymore controlled by phases that take up Cr into their octahedral sites but rather by Zr-enrichment in the liquid. As the tangent to the LLD approaches zero, small changes in the Cr-content of the liquid phase can be only attained by an escalation of the Zr-amount in the latter.

Ni-fractionation for the opaque-oxide gabbros appears to mimic the Cr-trend but with a wider range for the calculated results (Fig. 25 & 26). The outstanding sample (#13) does not show a representative modal volume and despite personal communication with R. Fodor (1990) the value in Table 1 of Fodor and Vandermeyden's publication (1990) might have been also subjected to typographical error. In summary, for Cr and Ni opaque oxide behaviour it can be shown that a considerable agreement was obtained for the calculated results and the analysed data. Yet, it is not possible to eliminate the fact that the calculated results are an effect of large changes in Zr-concentration for a small (ppms) change in Cr-content. Nevertheless, the high values of Zr could be also due to further evolution after "emplacement" of the host-hawaiite in the gabbros.

Unlike the two former trace elements Cr and Ni, Sr displays a somewhat ambigous behaviour when compared with Zr. For the olivine gabbroic assemblage in Fig. 21 & 22, the two Rayleigh fractionation curves were calculated with a $D^* < 1$. Fractionation of approximately 2 - 8 % plagioclase within the Hamakua lavas can account for the scattering of the volcanic data and allows to establish two different trends (TT & HT). In the model, the Sr bulk partition coefficient is less than one. However, it is evident that a large amount of Sr is still incorporated into the gabbros,

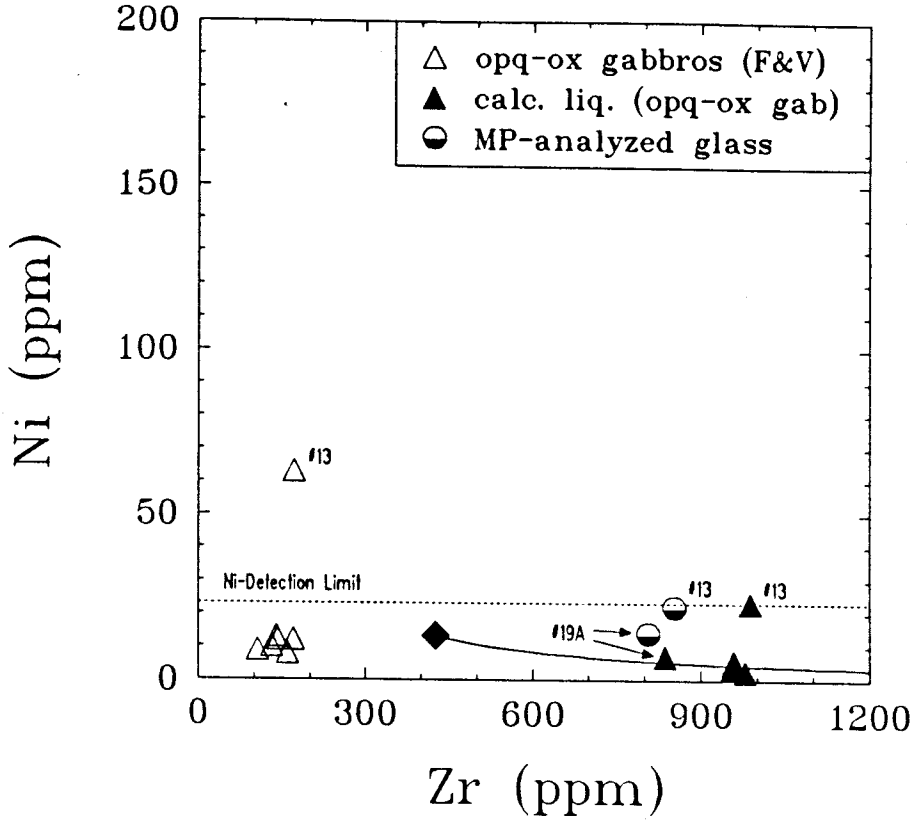

Fig. 25 : Ni against Zr for opaque-oxide gabbros. (extended model). 2 sigma error = 9 ppm for Ni and 3 ppm for Zr. Also, concentrations are only of qualitative value (see Fig. 24). Sample #13 does not show representative modal data according to Fodor and Vandermeyden (1988).

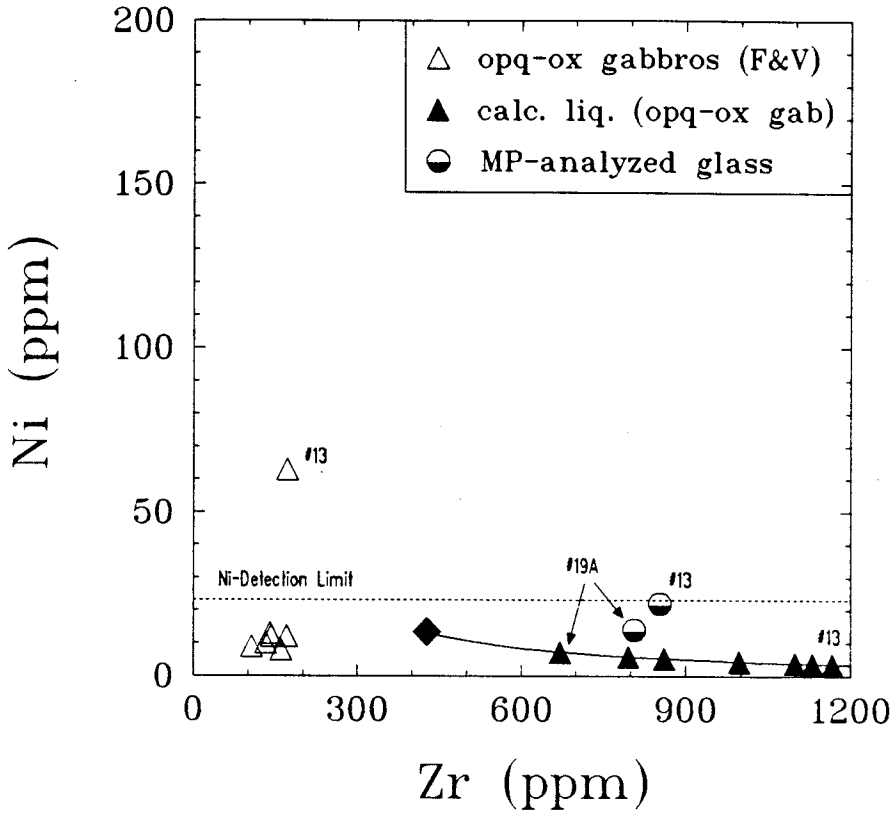

Fig. 26 : Ni against Zr for opaque-oxide gabbros. (single-pair). 2 sigma error = 9 ppm for Ni and 3 ppm for Zr.

increasing almost linearly with the growing amount of plagioclase in the samples. The widely spread data in Figure 21 reveal perfectly the difficulties in combining Cr, Ni, Sr and Zr distribution within a twodimensional geochemical framework. Since the bulk partition-coefficient for Sr is less than unity, a distinct path of fractionation can be easily obtained by a limited modification of the latter.

It has been shown in the discussion of the previous fractionation behaviour that a plausible explanation for the highly evolved glasses might be extended fractionation of the liquid phase that was brought into the gabbro by hawaiitic host-rock. Figure 27 shows a perfect positive correlation of K_2O and Zr enrichment in the fractionating liquid. The analysed glasses, the so called "trapped liquid component" occupy an end-member position in a trend that starts with low K_2O and low Zr in three gabbro samples #9, #13 and #19A. Selected values of the alkalic post-shield lavas (Frey et al., 1990 & West et al., 1988) fill the space along the trend between glass and gabbros. This nearly linear behaviour leads to the conclusion that the measured concentrations in the glass phase of the gabbros are in fact further fractionated liquid patches of the penetrating host rock. Perhaps, growth of mainly plagioclase and clinopyroxene and also minor opaque crystals within the liquid or advancement of these minerals from the surrounding phases into the liquid would have been sufficient to enrich the melt in the necessary amount of Zr.

This means for Figure 21, that due to a rough estimate the liquid must have continued in crystallizing approximately at least 60 % clinopyroxene with a $D^{cpx}_{Zr} = 2.3$ and 10 % plagioclase with a $D^{pl}_{Zr} = 1.65$ to reach the composition of the analyzed glass.

Looking at the single-pair model (Fig. 22), the calculated Laupahoehoe Trend results show a relative enrichment of Sr in the liquid. This phenomenon agrees well with the inference of Frey et al. (1990) that clinopyroxene was the first-crystallizing phase during the segregation of gabbroic cumulates at moderate pressure. Consequently, Laupahoehoe fractionation must have started with a high initial concentration for Sr.

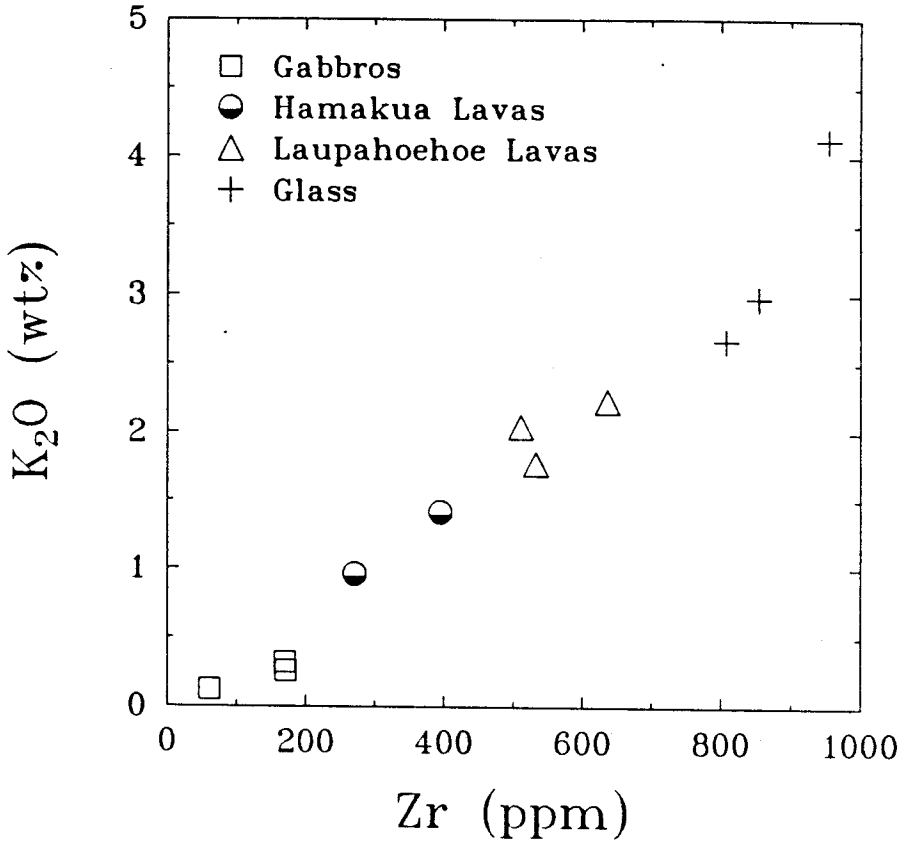

Fig. 27 : K_2O against Zr. Representative Hamakua and Laupahoehoe Lavas connect the "gap" between gabbros and evolved glass phase.

Partitioning of Sr into the gabbros during low-pressure fractionation causes a relative depletion in the cooling melt (Fig. 28 & 29). With the exception of two samples in Figure 28, of which one shows a relatively low modal volume of plagioclase, the computed data coincide with the expected numbers from the electron microprobe.

4.6 Sensitivity of model parameters

In contrast to the prior section in which the emphasis was put on the petrological context, this part tries to show the dependence of the model on starting compositions and partition-coefficients. Numerical experiments revealed that C^l_{Zr} and X^l are the most sensitive variables througout all calculations. Appendix C contains eight figures that display the numerical experiments with samples #2A and #19A. For sample #2A they show a variation from 30 - 50 % when
C^o_{Zr} ranges from 100 - 200 ppm. C^l_{Cr}, X^{φ} and F are relatively insensitive to changes in C^o_{Zr} (< 10 %). D* changes from -1.5 to -5 in sample #19A resulted in a range of 30 - 60 % deviation for C^l_{Zr} and 45 - 65 % for X^l. Considerable variance of C^l_{Zr} (up to 40 %), X^l (20 - 113 %) and also F (14 - 88) could be detected when C^o_{Cr} ranges from 3 to 15 ppm. Because of low absolute numbers, C^o_{Ni} showed minor variation during these tests while C^o_{Sr} varied from 1044 - 6711 ppm (42 - 78 %) with a change in C^o_{Cr} from 3 to 15 ppm.

4.7. Known modal volume of glass added as a single phase

Useful information is given by the modal data for the glass phase (that is obtained from Fodor and Vandermeyden's analysis, Table 1). By adding the modal volume to the known variables of the model, it is possible to reduce the number of assumed values by one. Thus, the mathematics become simplified because the iterative part of the calculations can be omitted (see appendix B for mathematical derivations). Arbitrarily,

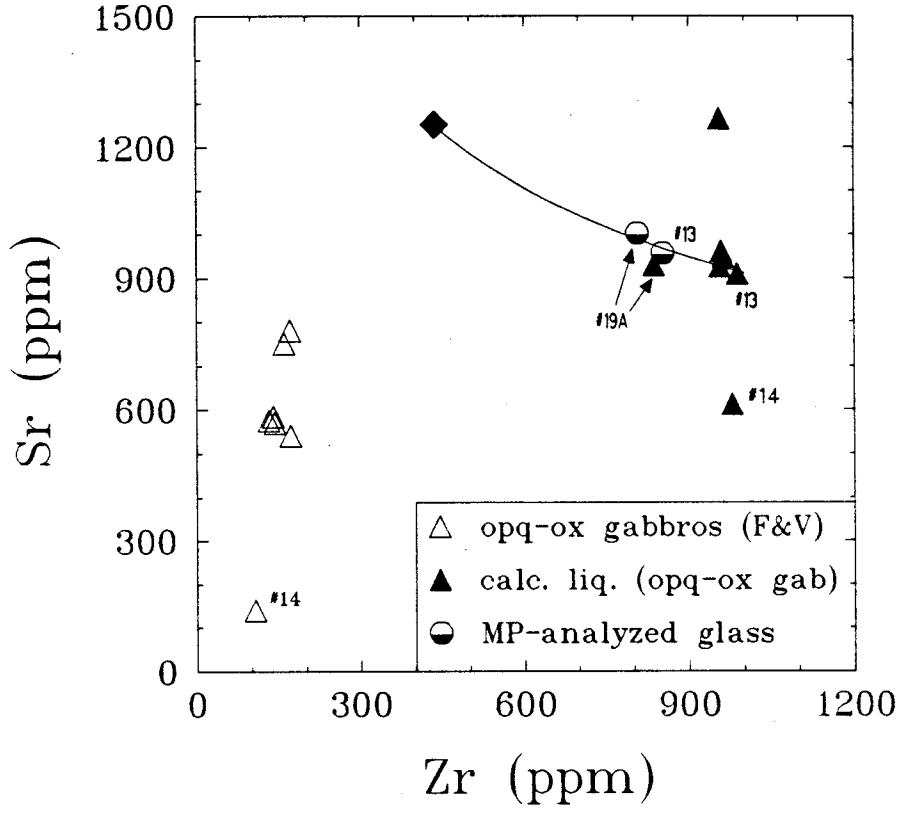

Fig. 28 : Sr against Zr for opaque-oxide gabbros (extended model). Sample #14 has an extremely high clinopyroxene content. For analyt. error of MP-glass see section 4.4.

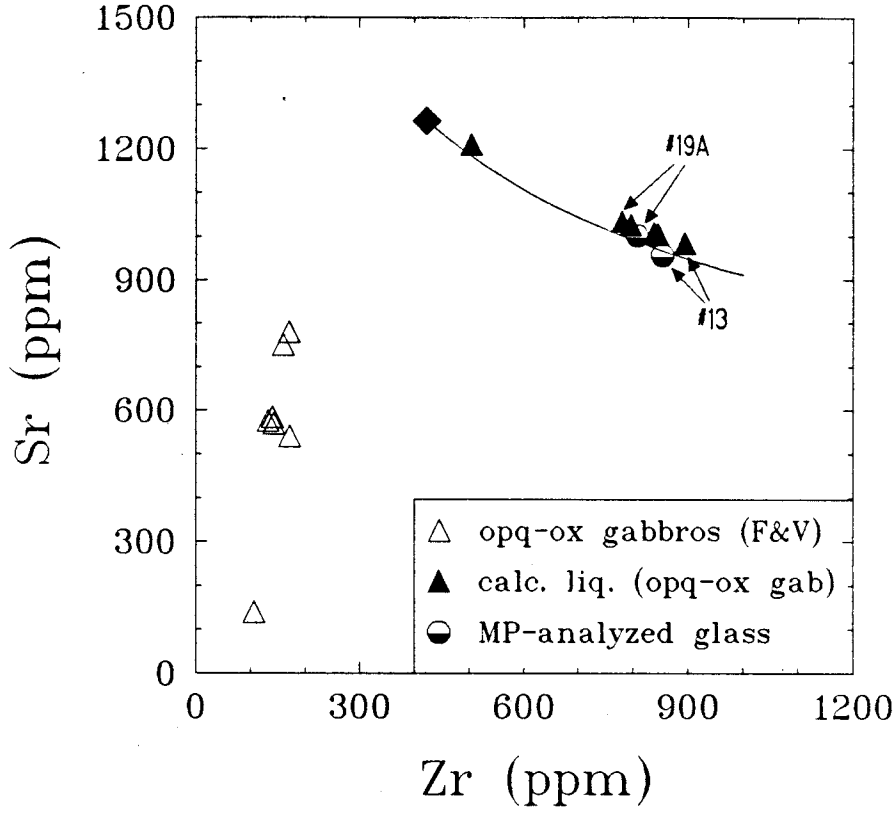

Fig. 29 : Sr against Zr for opaque-oxide gabbros (single-pair). For analyt. error of MP-glass see section 4.4.

sample 15B, an opaque-oxide gabbro, was chosen to use this simplified approach. Highly evolved liquid such as in sample 15B changes the Zr-content dramatically when the Cr-concentration is hardly modified. Therefor, it appears to be reasonable to set the Zr-value out of the two assumptions for the starting concentrations as a fixed number, and thus the Cr starting value can be calculated. The partition coefficients and C°_{Zr} are the same values as for the full iterative model when the modal amount of glass is unknown.

A comparison between these two approaches for sample 15B showed that the assumed value of C°_{Cr} versus the calculated value was shifted from 10.8 ppm to 70 ppm. In sample 15B the modal volume of the glass phase was found to be 0.2 %. This low amount of glass is responsible for an increase in Cr-concentration in the liquid to 70 ppm. To maintain a plausible value of Cr in the liquid with a starting concentration of 10.8 ppm, a modal glass volume of 8- 10 % would be required. Such a number is in good agreement with the weight-fraction computationally obtained from the extended model.

The sensitivity of the amount of glass to the behaviour of Cr-fractionation is a good example to show that the determination of the modal volume of a single thin section may not be representative of the bulk rock that was effectively averaged in the chemical analyses.

Chapter 5

5.1. Discussion

The quantitative results for this simple trace-element model that was applied to gabbroic xenoliths of Mauna Kea, Hawaii, are presented in Table V. Evidently, the TT olivine gabbros show the least evolved features with high F-values (0.7 - 0.76) and the lowest Zr-concentration in the liquid C^l_{Zr} (177 - 192 ppm), while the opaque-oxide gabbros definitely display a more evolved state with F-values of 0.42 - 0.5 and C^l_{Zr} of 836 - 987 ppm. An average F-value for the LT gabbros of 0.44 appears to be relatively close to values of West and others (1988) and Fodor and Vandermeyden (1989) who modelled major-elements that yielded a value for F = 0.4 and Frey and coworkers (1990) who calculated the amount of melt remaining in the chamber to be 0.5. Subtraction of a relatively plagioclase-poor, clinopyroxene-rich TT assemblage with F = 0.7 - 0.72 would produce a possible Laupahoehoe parent. However, to produce a gabbroic assemblage connected to the Hamakua Trend, an average of 60 % crystallization is necessary. This number appears to be quite different from the value obtained by Fodor and Vandermeyden, who modelled for both the Hamakua basalt and hawaiite an F of 0.7 - 0.75. This discrepancy might be explained on the one hand by the fact that Fodor and Vandermeyden did not really subdivide the olivine gabbros into two groups. Yet, the results of this study are strongly influenced by the choice of partition coefficients and starting compositions and a combination of input data and suitable model parameters would certainly allow a shift of F towards Fodor and Vandermeyden's value.

Two possible directions can be pursued when one is looking for the cause of inconsistencies between model and microprobe analyses, particularly for the concentrations of trace elements in the trapped liquid phase.

Focussing on the model itself, distribution coefficients and starting compositions

are, naturally, factors of uncertainty, a point that was discussed in a previous section. The mode of crystallization in the model, that is derived from the Rayleigh Fractionation Law for surface equilibrium, might be too simple to take into account more complicated patterns like periodic replenishment of the magma chamber, wall-rock assimilation or *in situ* crystallization near the margins of a magma-chamber. The latter was proposed by Fodor and Vandermeyden (1988) as a possible evolutionary history for the xenoliths (see chapter 3). However, *in situ* crystallized xenoliths would probably show randomly oriented grains, a wide range of grain sizes, strong zoning deep into the minerals and abundant intergrowth textures (Dixon et al., 1986). According to Fodor and Vandermeyden (1988), their description of the xenoliths does not support an origin of *in situ* crystallization. Nevertheless, too little is known about *in situ* crystallization so far and studies have been focussed rather on fluid dynamics and general crystallization processes than on complicated trace element behaviour.

A more plausible explanation for the inconsistencies between model output and glass analyses appears to originate from the question whether the latter are 'true' trapped liquid or simply host lava that penetrated the xenoliths. Arculus and Wills (1980) argued that crystals in contact with interstitial glass, found in plutonic blocks from lavas of the Lesser Antilles, show good development of euhedral crystals, a feature that is not observed at minerals of Mauna Kea xenoliths. Release of pressure and subsequent solution of minerals during ascent might give rise to force the liquid back into the rocks (Lewis, 1973), but no resorption and rare reaction features between the glass and the minerals of the xenoliths are found (Fodor and Vandermeyden, 1988). Flow structures in sample #19A might have been caused by stress either during accumulation of the cumulate pile or during transport to the surface.

Despite the fact that Cr and Ni analyses for opaque-oxide gabbros remain under the detection limit, it is possible to state qualitatively that a relative homogeneity of microprobe glass analyses for olivine and opaque-oxide gabbros is given because the

very low concentrations of compatible elements like Cr and Ni do not change significantly during evolution of late stage melts. Disequilibrium between melt and xenoliths (see 4.5.) corroborates the assumption that the 'trapped liquid' phase was created by the penetrating whole-rock. Also, higher evolved major elements for olivine gabbro glass than for opaque-oxide glass phases appear to originate from further evolution of the liquid after entrapment. Traces of host-lava in the gabbroic cumulates display features like colour and amount of phenocrystic material that are not consistent with the interstitial glass properties. The well correlated trend of K_2O against Zr in Fig. 27 clearly implies a tie between segregated gabbros, erupted volcanics and evolved 'trapped liquid'. Yet, it is hazardous to say that the liquid is definitely evolved host lava. Very small patches of melt (preferably melt inclusions) trapped within the cumulate pile might have developed such a high content of potassium and zirconium during evolution and further reaction with the surrounding minerals which lead to zoning in these crystals. No detailed studies were performed to investigate any mineral zonation patterns around the interstitial glass phase.

The ambiguity from petrographical observations as well as from geochemical studies makes it difficult to relate the trapped liquid phase strictly to one of the interpretations of Mauna Kea post-shield events that were presented in chapter 3. The segregated gabbroic assemblages can be reasonably related to the suggested low- and medium-p fractionation trends of Frey et al. (1990) and West et al. (1988). However, Fodor and Vandermeyden's suggestion of *in situ* crystallization cannot be fully excluded due to insufficient knowledge about the specific element partitioning in such a case.

5.2. Conclusions

1.) The model was tested successfully only for the opaque-oxide gabbros and within analytical error agreed with microprobe trace element analyses. Results for the olivine-gabbros did not agree with microprobe data of the glass phase.

2.) Predictions of Zr, Cr, Ni and Sr concentrations in the trapped liquid phase, weight fractions of mineral phases and the amount of magma remaining in the magma chamber did not further help to constrain the crystallization processes at Mauna Kea.

3.) Microprobe analyses of the glass phase display a highly fractionated state that might be consistent with further evolution of host lava that penetrated the gabbroic cumulates and carried them up to the surface.

4.) Studies of 'real' melt inclusions and zonation patterns of glass-surrounding minerals might be necessary to distinguish between host lava or true trapped liquid.

5.) Better knowledge of the general geological setting, i. e. a.) Are the erupted lavas real residual liquids of a fractionated cumulate gabbroic assemblage ? and b.) Is the liquid phase well enough defined to be 'trapped' during the accumulation of a plutonic assemblage? are of fundamental importance for the establishment of partition coefficients and starting compositions.

6.) Ion-microprobe analyses of clinopyroxene and the glass phase might give valuable results to check the significance of the selected partition coefficients (see appendix D).

References

Albarede, F. (1976) Some trace element relationships among liquid and solid phases in the course of the fractional crystallization of magmas. Geochim. Cosmochim. Act. 40, 667 - 673.

Arculus, R. K. and Wills, K. J. A. (1980) The petrology of plutonic blocks and inclusions from the Lesser Antilles Island Arc. J. Petrol. 21, 743 -799.

Barnes, S. J. (1986) The distribution of chromium among orthopyroxene, spinel and silicate liquid at atmospheric pressure. Geochim. Cosmochim. Act. 50, 1889 - 1909.

Bence, A. E. and Albee, A. L. (1967) Empirical correction factors for the electron microanalyses of silicates and oxides. J. Geol. 76, 382 - 403.

Bloomer, S. H., Natland, J. H. and Fisher, R. L. (1989) Mineral relationships in gabbroic rocks from fracture zones of Indian Ocean ridges: evidence for extensive fractionation, parental diversity and boundary-layer recrystallization; in: Magmatism in the ocean basins (ed. A. D. Saunders and M. J. Norry). Geol. Soc. Am. Spec. Publ. 42, 107-124.

Burns, R. G. (1973) The partitioning of trace transition elements in crystal structures: a provocative review with applications to mantle geochemistry. Geochim. Cosmochim. Act. 37, 2305 - 2403.

Clague, D. A. and Dalrymple, G. B. (1987) Hawaiian alkaline volcanism; in: Alkaline igneous rocks (ed. J. G. Fitton and B. G. Upton). Geol. Soc. Am. Spec. Publ. 30, 227-252.

Dixon, J. E., Clague, D. A. and Eissen, J. (1986) Gabbroic xenoliths and host ferrobasalt from the southern Juan de Fuca Ridge. J. Geophys. Res. 91, 3795 - 3820.

DeLong, S. E. and Chatelain, C. (1989) Complementary trace element fractionation in volcanic and plutonic rocks: imperfect examples from ocean-floor basalts and gabbros. Contrib. Mineral. Petrol. 102, 154 - 162.

Drake, M. J. and Weill, D. F. (1975) Partitioning of Sr, Ba, Ca, Y, Eu^{2+}, Eu^{3+} and other REE between plagioclase feldspar and magmatic liquid: an experimental study. Geochim. Cosmochim. Act. 39, 689 - 712.

Elthon, D. (1987) Petrology of gabbroic rocks from the Mid-Cayman Rise spreading center. J. Geophys. Res. 92, 658 - 682.

Frey, F. A., Wise, W. S., Garcia, M. O., West, H., Kwon, S.-T. and Kennedy, A. (1990) Evolution of Mauna Kea Volcano, Hawaii: Petrologic and geochemical constraints on postshield volcanism. J. Geophys. Res. 95, 1271-1300.

Fodor, R. V. and Vandermeyden, H. J. (1988) Petrology of gabbroic xenoliths from Mauna Kea, Hawaii. J. Geophys. Res. 93, 4435 - 4452.

Griffin, W. L. and Murthy, V. R. (1969) Distribution of K, Rb, Sr and Ba in some minerals relevant to basalt genesis. Geochim. Cosmochim. Act. 33, 1389 - 1414.

Hart, S. R. and Brooks, C. (1974) Clinopyroxene-matrix partitioning of K, Rb, Sr and Ba. Geochim. Cosmochim. Act. 38, 1799 - 1806.

Hart, S. R. and Davis, K. E. (1978) Nickel partitioning between olivine and silicate melt. Earth Planet. Sci. Lett. 40, 203 - 219.

Hodges, F, N. and Papike, J. J. (1976) DSDP site 34: magmatic cumulates from oceanic layer 3. J. Geophys. Res. 81, 4135 - 4151.

Huebner, J. S., Lipin, B. R. and Wiggins, L. B. (1976) Partitioning of chromium between silicate crystals and melt. Proc. Lunar Sci. Conf. 7th, 1195 - 1220.

Irving, A. J. (1978) A review of experimental studies of crystal/liquid trace element partitioning. Geochim. Cosmochim. Act. 42, 743 - 770.

Irving, A. J. and Frey, F. A. (1984) Trace element abundances in megacrysts and their host basalts: Constraints on partition coefficients and megacryst genesis. Geochim. Cosmochim. Act. 48, 1201 - 1221.

Kinzler, R. J., Grove, T. L. and Recca, S. I. (1990) An experimental study on the effect of temperature and melt composition on the partitioning of nickel between olivine and silicate melt. Geochim. Cosmochim. Act. 54, 1255 - 1265.

Korringa, M. K. and Noble, D. C. (1971) Distribution of Sr and Ba between natural feldspar and igneous melt. Earth Planet. Sci. Lett. 11, 147 - 151.

Leeman, W. P. and Lindstrom, D. J. (1978) Partitioning of Ni^{2+} between basaltic and synthetic melts and olivines - an experimental study. Geochim. Cosmochim. Act. 42, 801 - 816.

Lewis, J. F. (1973) Petrology of the ejected plutonic blocks of the Soufriere Volcano, St. Vincent, West Indies. J. Petrol. 4, 81 - 112.

Lindstrom, D. J. and Weill, D. F. (1978) Partitioning of transition metals between diopside and coexisting silicate liquids. I. nickel, cobalt and manganese. Geochim. Cosmochim. Act. 42, 817 - 831.

Mahood, G. A. and Baker, D. R. (1986) Experimental constraints on depths of fractionation of mildly alkalic basalts and associated felsic rocks: Pantellieria, Straight of Sicily. Contrib. Mineral. Petrol. 93, 251-269.

MacDonald, G. A. and Katsura, T. (1964) Chemical composition of Hawaiian Lavas. J. Petrol. 5, 82-133

McBirney, A. R. and Noyes, R. M. (1979) Crystallization and layering of the Skaergaard intrusion. J. Petrol. 20, 487 - 554

McIntire, W. L. (1963) Trace element partition coefficients - review of theory and

Miyashiro, A., Shido, F. and Ewing, M. (1970) Crystallization and differentiation in abyssal tholeiites and gabbros from mid-ocean ridges. Earth Planet. Sci. Lett. 7, 361-365.

Pearce, J. A. and Norry, M. J. (1979) Petrogenetic implications of Ti, Zr, Y and Nb variations in volcanic rocks. Contrib. Mineral. Petrol. 69, 33 - 47.

Philpotts, J. A. and Schnetzler, C. C. (1970) Phenocryst-matrix partition coefficients for K, Rb, Sr and Ba, with application to anorthosite and basalt genesis. Geochim. Cosmochim. Act. 34, 307 - 322.

Roeder, P. L. and Emslie, R. F. (1970) Olivine-liquid equilibrium. Contr. Mineral. Petrol. 29, 275 - 289.

Stroup, J. B., Malcolm, F. L. and Spydell, R. (1978) Petrology of submersible collected plutonic rocks from the Cayman trough, Caribbean (abstract). EOS Trans. AGU 59, 405.

Sun, C-O., Williams, R. J. and Sun, S-S. (1974) Distribution coefficients of Eu and Sr for plagioclase-liquid and clinopyroxene-liquid equilibria in oceanic-ridge basalts: an experimental study. Geochim. Cosmochim. Act. 38, 1415 - 1433.

Thompson, G., Bryan, W. B. and Melson, W. G. (1978) Geochemical variations and petrogenesis of basalt glass from the Cayman Trough spreading center. EOS Trans. AGU 59, 405.

Tiezzi, L. J. and Scott, R. B. (1980) Crystal fractionation in a cumulate gabbro, MAR 25^{o} N. J. Geophys. Res. 85, 5438-5454.

Vandermeyden, H. J. (1985) Petrology of gabbroic xenoliths from the summit cone of Mauna Kea Volcano, Hawaii. Master thesis, North Carolina State University at Raleigh.

Watson, E. B. and Harrison, T. M. (1984) Accesory minerals and the geochemical evolution of crustal magmatic systems: a summary and prospectus of experimental approaches. Phys. Earth Planet. Int. 35, 19 - 30.

West, H. B., Garcia, M. O., Frey, F. A. and Kennedy A. (1988) Nature and cause of compositional variation among the alkalic cap lavas of Mauna Kea Volcano, Hawaii. Contrib. Mineral. Petrol. 100, 383-397.

Wood, B. J. and Fraser D. G. (1977) Elementary thermodynamics for geologists. Oxford University Press, 303 pp.

Appendix A

The computer-programm, written in FORTRAN, calculates F, Crl, Zrl, Nil, Srl, Xl, Xcpx, Xol, Xpl, Xspl, Xopq, Xap, Nio and Sro. Zrl and Crl are obtained by an iterative process (see section "Iteration by Bisection Method" in the program) and are used to calculate the other unknowns in program-section "Final Formulas for Remaining Unknowns.

```
**************************************************************

      program TRACEALL

C****DEFINITION OF VARIABLES

C     CM - chromium
C     SPL - chromium-bearing oxides
C     LEFTERM, RIGHTERM - both terms of eq. (34) represent
C     chromium concentration in the liquid phase
C     CMO - chromium starting concentration in magma
C     ZRL - concentration of Zr in the liquid phase
C     (the two expressions above are analogous for the other
C     elements)

C**************************************************************

C****DECLARATION OF VARIABLES

      REAL M1,M2,M3,M4,M5,NI,LEFTERM,NIL

      CHARACTER NAME *10

C**************************************************************

C****DISTRIBUTION COEFFICIENTS

C     (there are three sets of distribution coefficients,
C     that can be selectively exchanged to fit a specific
C     fractionation trend. See table II and V for other
      options.)


      DCPXCM=13
      DOLCM=1.1
      DPLCM=0.02
      DSPLCM=2.0
      DOPQCM=10
      DAPCM=0.01
      DCPXZR=0.15
      DOLZR=0.01
      DPLZR=0.01
      DSPLZR=0.1
```

```
      DOPQZR=0.02
      DAPZR=0.01
      DCPXNI=6
      DOLNI=15
      DPLNI=0.06
      DSPLNI=4
      DOPQNI=1.5
      DAPNI=0.2
      DCPXSR=0.11
      DOLSR=0.'014
      DPLSR=1.35
      DSPLSR=0.01
      DOPQSR=0.01
      DAPSR=2

C*************************************************************

C****DATA-INPUT

      PRINT*,'SAMPLE ID'
      READ(*,'(A)')NAME

      PRINT*,'CM-CONTENT'
      READ*,CM
      PRINT*,'ZR-CONTENT'  ! *** gabbro Zr-content
      READ*,ZR
      PRINT *,'NI-CONTENT' ! ***gabbro Ni-content
      READ*,NI
      PRINT*,'SR-CONTENT'  ! ***gabbro Sr-content
      READ*,SR

      PRINT*,'OL-CONTENT'  ! *** mode (volume%)
      READ*,OL
      PRINT*,'CPX-CONTENT' ! *** mode (volume%)
      READ*,CPX
      PRINT*,'PL-CONTENT'  ! *** mode (volume%)
      READ*,PL
      PRINT*,'SPL-CONTENT'  ! *** mode (volume%)
      READ*,SPL
      PRINT*,'AP-CONTENT'  ! *** mode (volume%)
      READ*,AP
      PRINT*,'OPQ-CONTENT' ! *** mode (volume%)
      READ*,OPQ

C*************************************************************

C****STARTING CONDITIONS

      PRINT*,'WHICH STARTING VALUE?'
      PRINT*,'HAMAKUA = 1     LAUPAHOEHOE = 2
&                TRANSITION = 3'

      READ*,ISET
```

```
      IF (ISET.EQ.1) THEN
      DZR=0.02 ! *** bulk D
      DCM=2.92 ! *** ditto
      ZRO=135
      CMO=1167
      DSTAR=1.95 ! *** (Dcm-1)/(Dzr-1)

      ELSEIF (ISET.EQ.2) THEN
      DZR=0.02
      DCM=3.35
      ZRO=425
      CMO=10.8
      DSTAR=2.4

      ELSE
      DZR=0.02
      DCM=4.72
      ZRO=135
      CMO=1167
      DSTAR=3.8
      ENDIF

C*************************************************************

      M1=1.222*CPX/PL  ! *** density normalization
      M2=1.259*OL/PL
      M3=1.556*SPL/PL
      M4=1.778*OPQ/PL
      M5=1.185*AP/PL

      ALPHACM1=(M1*DCPXCM+DPLCM+M2*DOLCM+M3*DSPLCM+M4*DOPQM
     &          +M5*DAPCM)
      ALPHACM2=(1+M1+M2+M3+M4+M5)
      ALPHACM3=ALPHACM1/ALPHACM2

      ALPHAZR1=(M1*DCPXZR+DPLZR+M2*DOLZR+M3*DSPLZR+M4*DOPQZR
     &          +M5*DAPZR)
      ALPHAZR2=(1+M1+M2+M3+M4+M5)
      ALPHAZR3=ALPHAZR1/ALPHAZR2

      ALPHANI1=(M1*DCPXNI+DPLNI+M2*DOLNI+M3*DSPLNI+M4*DOPQNI
     &          +M5*DAPNI)
      ALPHANI2=(1+M1+M2+M3+M4+M5)
      ALPHANI3=ALPHANI1/ALPHANI2

      ALPHASR1=(M1*DCPXSR+DPLSR+M2*DOLSR+M3*DSPLSR+M4*DOPQSR
     &          +M5*DAPSR)
      ALPHASR2=(1+M1+M2+M3+M4+M5)
      ALPHASR3=ALPHASR1/ALPHASR2

      R1=(1-ALPHACM3)/(1-ALPHAZR3)
      R2=(1-ALPHACM3)/(1-ALPHANI3)
      R3=(1-ALPHACM3)/(1-ALPHASR3)
```

```
C*************************************************************
C****ITERATION BY BISECTION-METHOD

      EPS=0.01   ! *** error tolerance for iteration
      IMAX=100   ! *** maximum number of iteration permitted


      PRINT*,'LOWER LIMIT OF ZRL =?'
      READ*,ZRLOW
      PRINT*,'UPPER LIMIT OF ZRL =?'
      READ*,ZRLUP

      LEFTERM=CM/(R1*(ZR/ZRLOW-ALPHAZR3)+ALPHACM3) ! *** Cm-
C     content in liq
      RIGHTERM=CMO/(ZRLOW/ZRO)**DSTAR ! *** ditto
      FLOW=RIGHTERM-LEFTERM

      LEFTERM=CM/(R1*(ZR/ZRLUP-ALPHAZR3)+ALPHACM3) ! *** Cm-
C     Content in liq
      RIGHTERM=CMO/(ZRLUP/ZRO)**DSTAR ! *** ditto
      FUP=RIGHTERM-LEFTERM

      SIGNFLOW=SIGN(1.,FLOW)
      SIGNFUP=SIGN(1.,FUP)

      IF (SIGNFLOW.EQ.SIGNFUP)THEN
      PRINT*,'NO SOLUTION WITHIN CHOSEN LIMITS'
      STOP
      ENDIF

      I=1
200   CONTINUE

      ZRLNEW=(ZRLOW+ZRLUP)/2
      CHNGE=ZRLNEW-ZRLOW

      LEFTERM=CM/(R1*(ZR/ZRLNEW-ALPHAZR3)+ALPHACM3) ! *** Cm-
C     content in liq
      RIGHTERM=CMO/(ZRLNEW/ZRO)**DSTAR ! *** ditto
      FNEW=RIGHTERM-LEFTERM

      SIGNFNEW=SIGN(1.,FNEW)

      IF (SIGNFNEW.EQ.SIGNFUP)THEN
      ZRLUP=ZRLNEW
      SIGNFUP=SIGNFNEW
      ELSE
      ZRLOW=ZRLNEW
      SIGNFLOW=SIGNFNEW
      ENDIF
```

```
C****CHECK IF ITERATION CAN BE FINISHED

      IF((ABS(CHNGE).LT.EPS).OR.(FNEW.EQ.0.))THEN

      ZRL=ZRLNEW   ! *** solution is found
C****solution for ZRL

C     CML=LEFTERM
C****solution for CML


      GOTO 300

      ELSE

C****CHECK IF MAX. NUMBER OF ITERATIONS ARE EXCEEDED

      IF(I.GT.IMAX)THEN
      PRINT*,'NO SOLUTION AFTER',I,'ITERATIONS'
      STOP

      ELSE
      I=I+1
      GOTO 200

      ENDIF
      ENDIF

300   CONTINUE

C*************************************************************

C****FINAL FORMULAS FOR REMAINING UNKNOWNS

      F=(LEFTERM/ZRL/(CMO/ZRO))**(1/(DCM-DZR)) ! *** fraction
C     of residual magma
      NIL=NI*(R2/(CM/LEFTERM+R2-1)) ! *** Ni content in
C     liquid
      SRL=SR*(R3/(CM/LEFTERM+R3-1)) ! *** Sr content in
C     liquid
      XL=(CM/LEFTERM-ALPHACM3)/(1-ALPHACM3) ! *** liq-
C     fraction in gabbro
      XPL=(1-XL)/(1+M1+M2+M3+M4+M5)
      XCPX=M1*XPL
      XOL=M2*XPL
      XSPL=M3*XPL
      XOPQ=M4*XPL
      XAP=M5*XPL
      NIO=NIL/((ZRL/ZRO)**(DSTARN)) ! *** Ni starting
C     concentration
      SRO=SRL*((ZRL/ZRO)**(DSTARS)) ! *** Sr starting
C     concentration
```

```
C*****************************************************************

C****DATA OUTPUT

      PRINT*,' '
      PRINT*,'SAMPLE= ',NAME
      PRINT*,'ITERATIONS= ',I
      PRINT*,' '
      PRINT*,'STARTING VALUES',ISET
      PRINT*,'ZRO=',ZRO,      'CMO=',CMO
      PRINT*,'NIO=',NIO,      'SRO=',SRO
      PRINT*,'DSTAR= ',-DSTAR
      PRINT*,' '
      PRINT*,'ZR=',ZR,'       CM=',CM
      PRINT*,'PL(VOL%)=',PL,' CPX(VOL%)=',CPX
      PRINT*,'OL(VOL%)=',OL,' SPL(VOL%)=',SPL
      PRINT*,'AP(VOL%)=',AP,' OPQ(VOL%)=',OPQ
      PRINT*,' '
      PRINT*,'F LIQ=',F,'   ZR LIQ=',ZRL
      PRINT*,' '
      PRINT*,'CM LIQ=',LEFTERM,'  NI LIQ=',NIL,'  SR
     1       LIQ=',SRL
      PRINT*,' '
      PRINT*,'X LIQ=',XL,'   X PLAG=',XPL,'   X CPX=',XCPX
      PRINT*,' '
      PRINT*,'X SPL=',XSPL,'    X OL=',XOL,'     X AP=',XAP
      PRINT*,' '
      PRINT*,'X OPQ=',XOPQ
      END
```

Appendix B

If we now take the liquid phase as a known component of the cumulate (observed as displayed in the modal data of Fodor and Vandermeyden, 1988), we can add another mass-fraction to the equations in appendix A. Thus, obtaining fifteen equations for the already existing sixteen unknown parameters, only a single assumption for the starting compositions has to be made. C^{o}_{Cr} is favoured because this number vigorously determines the fractionation trend of the liquid. The fifteen equations are:

$$C^{l}_{Cr} = C^{o}_{Cr} F^{D_{Cr}-1} \tag{B.1}$$

$$C^{l}_{Zr} = C^{o}_{Zr} F^{D_{Zr}-1} \tag{B.2}$$

$$C^{l}_{Ni} = C^{o}_{Ni} F^{D_{Ni}-1} \tag{B.3}$$

$$C^{l}_{Sr} = C^{o}_{Sr} F^{D_{Sr}-1} \tag{B.4}$$

$$X^{l} + X^{cpx} + X^{ol} + X^{pl} + X^{spl} + X^{opq} + X^{ap} = 1 \tag{B.5}$$

$$\frac{C^{gab}_{Cr}}{C^{l}_{Cr}} = X^{l} + X^{cpx}D^{cpx/l}_{Cr} + X^{ol}D^{ol/l}_{Cr} + X^{pl}D^{pl/l}_{Cr} + X^{spl}D^{spl/l}_{Cr} + X^{opq}D^{opq/l}_{Cr} + X^{ap}D^{ap/l}_{Cr} \tag{B.6}$$

$$\frac{C^{gab}_{Zr}}{C^{l}_{Zr}} = X^{l} + X^{cpx}D^{cpx/l}_{Zr} + X^{ol}D^{ol/l}_{Zr} + X^{pl}D^{pl/l}_{Zr} + X^{spl}D^{spl/l}_{Zr} + X^{opq}D^{opq/l}_{Zr} + X^{ap}D^{ap/l}_{Zr} \tag{B.7}$$

$$\frac{C^{gab}_{Ni}}{C^{l}_{Ni}} = X^{l} + X^{cpx}D^{cpx/l}_{Ni} + X^{ol}D^{ol/l}_{Ni} + X^{pl}D^{pl/l}_{Ni} + X^{spl}D^{spl/l}_{Ni} + X^{opq}D^{opq/l}_{Ni} + X^{ap}D^{ap/l}_{Ni} \tag{B.8}$$

$$\frac{C^{gab}_{Sr}}{C^{l}_{Sr}} = X^{l} + X^{cpx}D^{cpx/l}_{Sr} + X^{ol}D^{ol/l}_{Sr} + X^{pl}D^{pl/}_{Sr} + X^{spl}D^{spl/l}_{Sr} + X^{opq}D^{opq/l}_{Sr} + X^{ap}D^{ap/l}_{Sr} \qquad (B.9)$$

$$M_1 = \frac{X^{cpx}}{X^{pl}} = \frac{\rho^{cpx}\, V^{cpx}}{\rho^{pl}\, V^{pl}} \qquad (B.10)$$

$$M_2 = \frac{X^{ol}}{X^{pl}} = \frac{\rho^{ol}\, V^{ol}}{\rho^{pl}\, V^{pl}} \qquad (B.11)$$

$$M_3 = \frac{X^{spl}}{X^{pl}} = \frac{\rho^{spl}\, V^{spl}}{\rho^{pl}\, V^{pl}} \qquad (B.12)$$

$$M_4 = \frac{X^{opq}}{X^{pl}} = \frac{\rho^{opq}\, V^{opq}}{\rho^{pl}\, V^{pl}} \qquad (B.13)$$

$$M_5 = \frac{X^{ap}}{X^{pl}} = \frac{\rho^{ap}\, V^{ap}}{\rho^{pl}\, V^{pl}} \qquad (B.14)$$

$$M_6 = \frac{X^{l}}{X^{pl}} = \frac{\rho^{l}\, V^{l}}{\rho^{pl}\, V^{pl}} \qquad (B.15)$$

The relative mass fractions, Eq. (B.10 - B.15.), are combined with (B.5), respectively, resulting in

$$X^{cpx} = \frac{M_1}{1 + M_1 + M_2 + M_3 + M_4 + M_5 + M_6} \qquad (B.16)$$

$$X^{ol} = \frac{M_2}{1 + M_1 + M_2 + M_3 + M_4 + M_5 + M_6} \qquad (B.17)$$

$$X^{pl} = \frac{1}{1 + M_1 + M_2 + M_3 + M_4 + M_5 + M_6} \qquad (B.18)$$

$$X^{spl} = \frac{M3}{1 + M1 + M2 + M3 + M4 + M5 + M6} \quad (B.19)$$

$$X^{opq} = \frac{M4}{1 + M1 + M2 + M3 + M4 + M5 + M6} \quad (B.20)$$

$$X^{ap} = \frac{M5}{1 + M1 + M2 + M3 + M4 + M5 + M6} \quad (B.21)$$

$$X^{l} = \frac{M6}{1 + M1 + M2 + M3 + M4 + M5 + M6} \quad (B.22)$$

Eq. (B.16 - B.22) can be coupled with Eq. (B.6), and after rearrangement results in similar equations for four different elements ξ, respectively:

$$\frac{C_\xi^{gab}}{C_\xi^{l}} = \alpha_\xi \quad (B.23)$$

where

$$\alpha_\xi = \frac{M1D_\xi^{cpx/l} + M2D_\xi^{ol/l} + D_\xi^{pl/l} + M3D_\xi^{spl/l} + M4D_\xi^{opq/l} + M5D_\xi^{ap/l} + M6}{1 + M1 + M2 + M3 + M4 + M5 + M6} \quad (B.24)$$

Out of Eq. (B.23), the concentration of each element Cr, Zr, Ni and Sr in the liquid can be obtained very easily, and by the same final procedure as in Appendix A the other parameters are found.

Appendix C

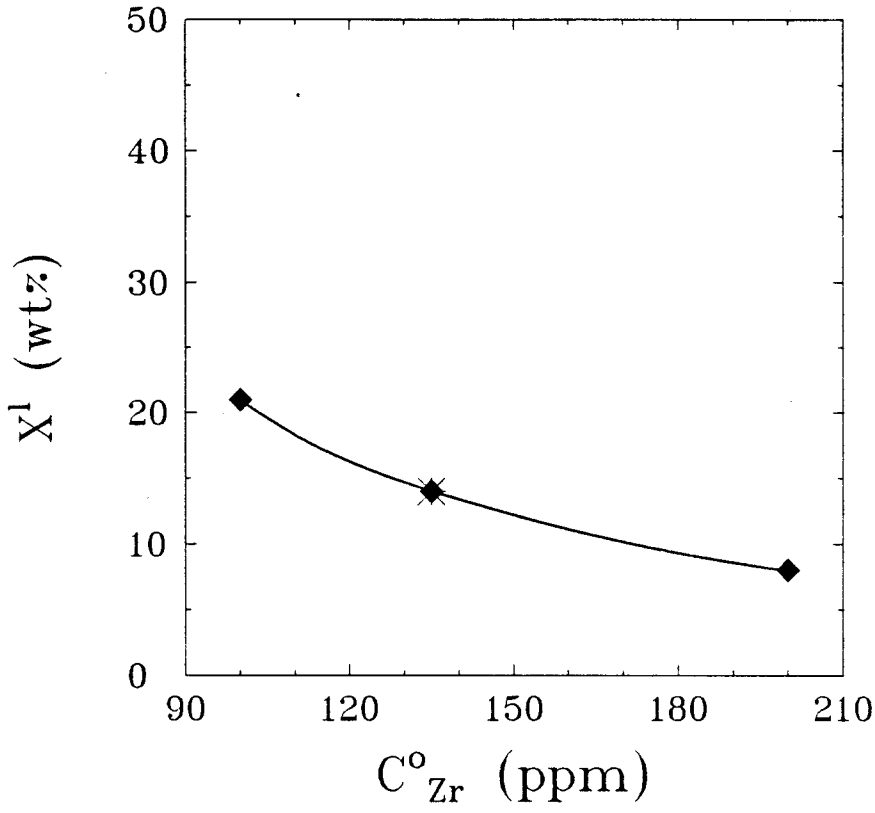

sensitivity test for sample #2A

variation of Zro : 100 -. 200 ppm

✱ = calculated result for #2A

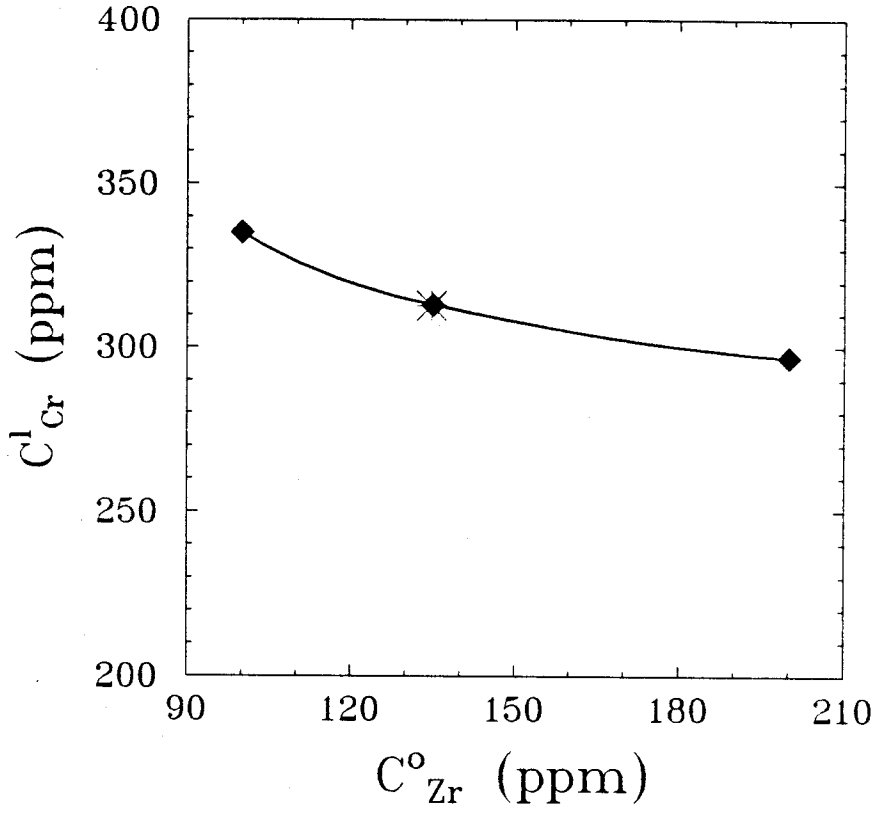

sensitivity test for sample #2A

variation of Zro : 100 - 200 ppm

◆ = calculated result for #2A

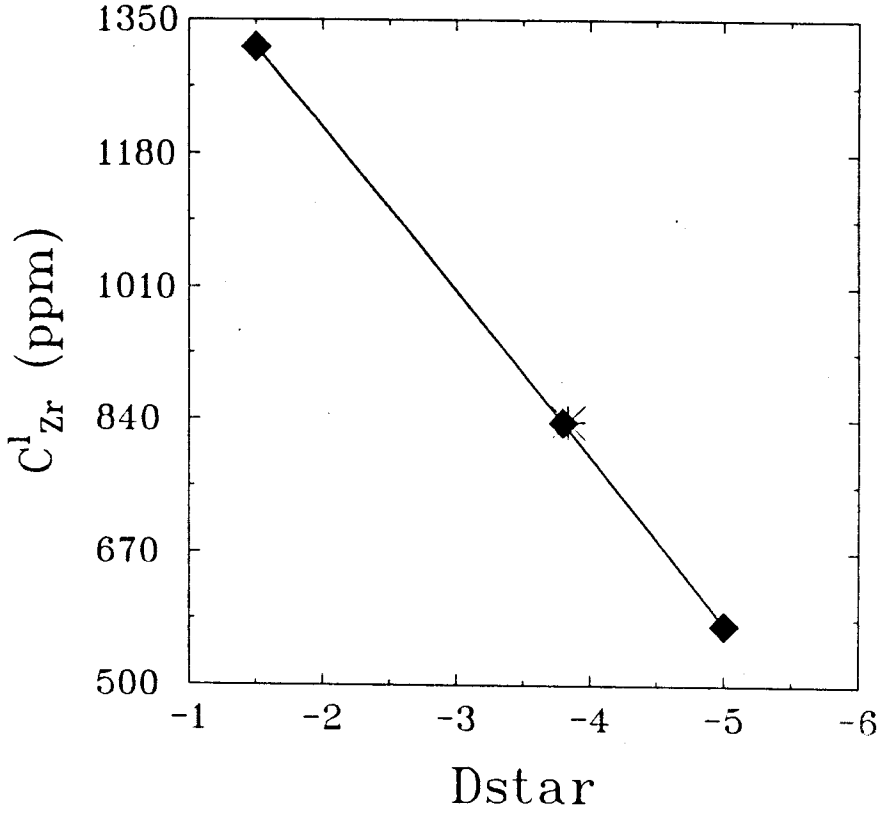

sensitivity test for sample #19A

variation of Dstar : -1.5 - -5.0

◆ = calculated result for #19A

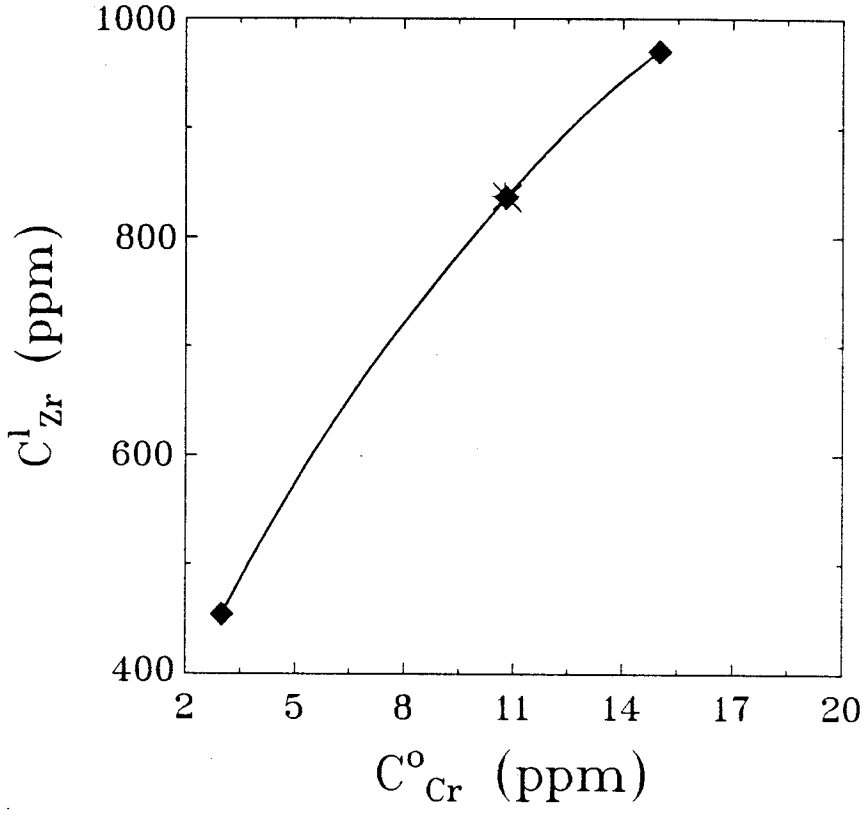

sensitivity test for sample #19A

variation of Cro : 3 - 15 ppm

✱ = calculated result for #19A

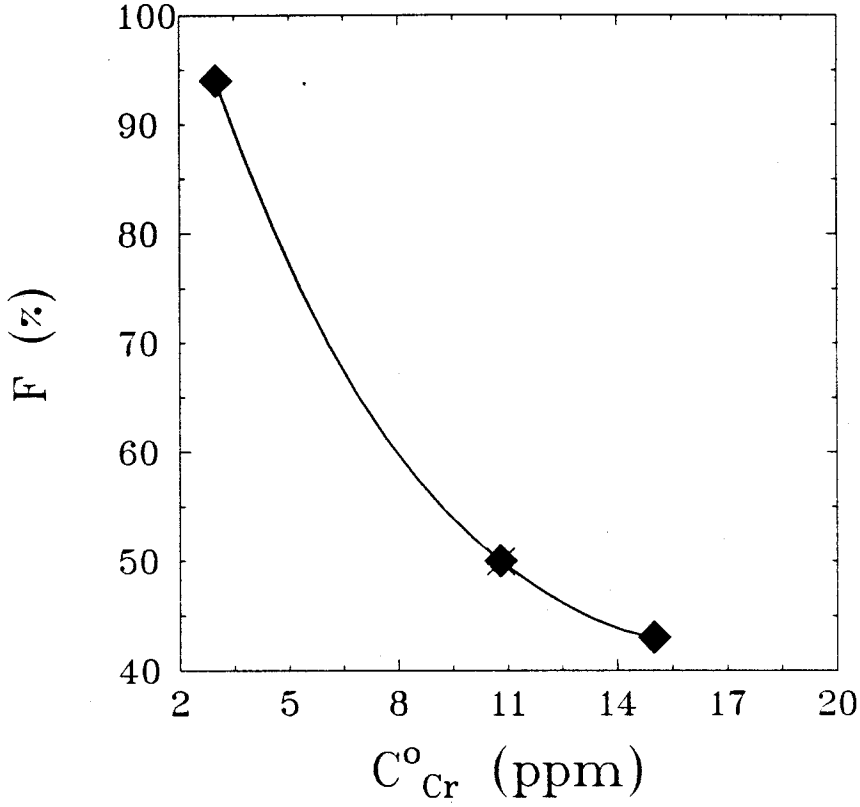

sensitivity test for sample #19A

variation of Cro : 3 - 15 ppm

✱ = calculated result for #19A

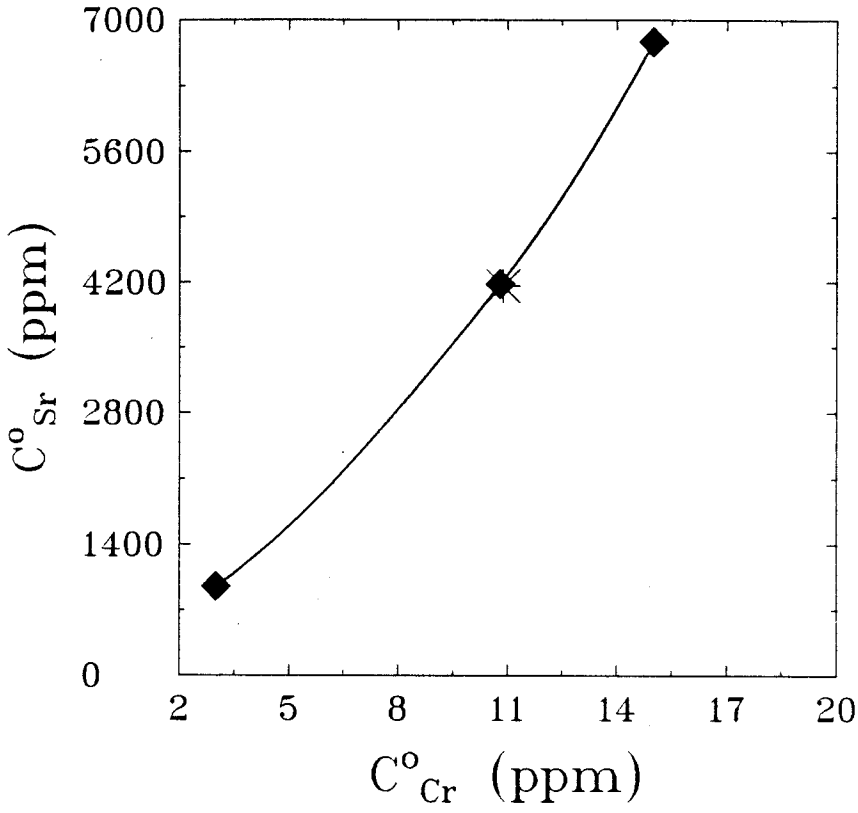

sensitivity test for sample #19A

variation of Cro : 3 - 15 ppm

= calculated result for #19A

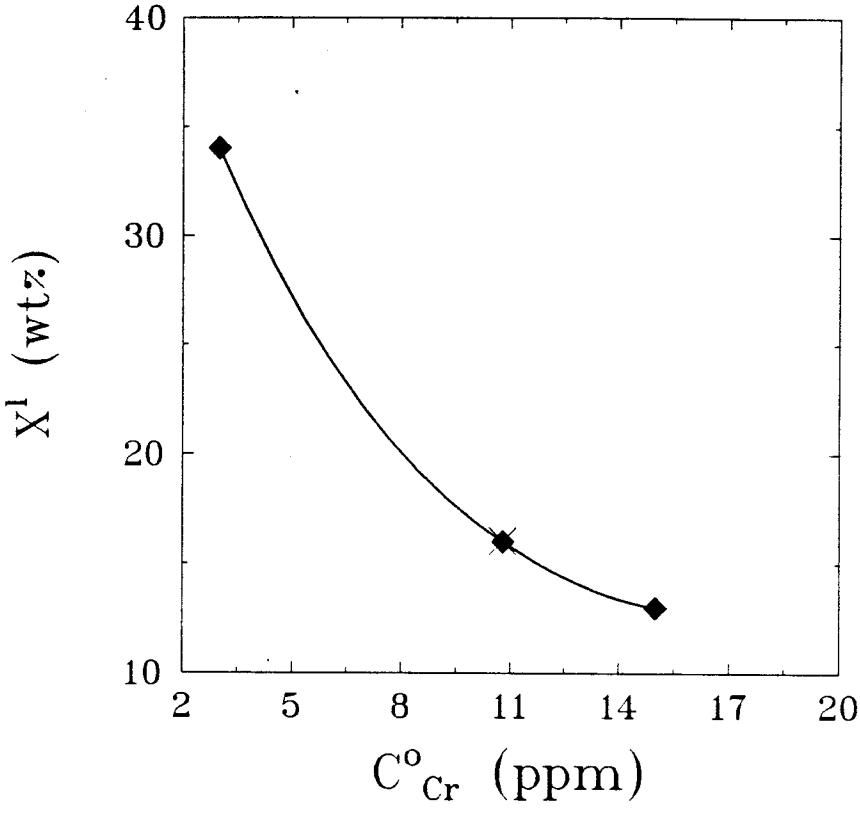

sensitivity test for sample #19A

variation of Cro : 3 - 15 ppm

✱ = calculated result for #19A

Appendix D

After the main work of this study was done, I obtained the opportunity to get additional analyses from the ion microprobe at Woods Hole Oceanographic Institution.

Sample #13, #19A and #9 were analyzed for REE and trace elements such as Cr, Zr, Sr. A primary beam with an 1-2 nA current and a net energy of ≈ 12 keV was focused on a spot of ≈ 20 μm. Precision of data and overall accuracy is believed to be ± 5 - 10 % for Cr and, ± 10 - 15 % for Sr and Zr, ± 10 - 25 % for LREE and ± 10 - 15 % for middle and heavy REE (Johnson et al., 1990).

Table D1 displays the trace element analyses for Cr, Sr and Zr and the respective partition coefficients between cpx and the glass phase for sample #13 (LT) and #9 (TT). Trace element concentrations are close to those numbers measured at the electron microprobe (table VI, p. 43). The ion microprobe partition coefficients between cpx and glass, $D^{cpx/l}$, for those two samples and the assumed $D^{cpx/l}$ for the model (table II, p. 30) appear to show a relative conformity for Sr and Zr within analytical error. The Cr-partition coefficients for sample #9 (TT) exceeds the assumed value by a factor of ten which might be due to the fact that the beam was not focussed on an inclusion-free spot in the cpx or also, the glass might be in disequilibrium with its adjacent cpx.

REE general patterns (Fig. D1) and REE single runs (Fig. D2) for sample #13, #19A and #9 suggest a state of equilibrium from their similar glass and cpx patterns. Those two patterns are complementary in the way that LREE are enriched in the glass while they are depleted in cpx. The calculated partition coefficien shown in table DIII are compared with partition coefficients form the literure (table DIV Relatively conformable numbers appear to indicate equilibrium conditions for glass and cpx in sample #9 and #19A. The average results for #13 as well as the single runs are higher than the data from the literature.

Table DI Ion-microprobe trace element analyses of glass and cpx in gabbroic xenoliths and their partition coefficients

sample#	Cr	Sr	Zr
glass			
9-1	41	769	1138
13-1	10	669	962
cpx			
9-1	5506	68	43
13-1	207	70	135
Dcpx/glass			
9-1	134.29	0.09	0.04
13-1	20.70	0.10	0.14

Table DII Ion-Microprobe REE analyses (chondrite normalized) of glass and cpx in gabbroic xenoliths

sample #	La	Ce	Nd	Sm	Eu	Dy	Er	Yb
glass								
13-4	380	315	217	180	94	100	74	50
13-1/2	175	125	107	116	65	54	32	24
13-3	216	158	127	108	55	59	41	28
19A-1	103	72	62	66	36	31	17	13
9-1	99	67	49	48	26	21	13	10
cpx								
13-4	70	85	99	104	35	59	38	25
13-1/2	43	46	60	66	20	39	24	19
13-3	23	27	40	48	17	31	18	14
19A-1	6.9	7.9	14	25	10	13	5.6	4.6
9-1	2.9	3.2	5.7	10	4.2	5.5	2.5	2.1

Table DIII Partition coefficients calculated from ion-microprobe data (concentration in cpx / concentration in glass)

sample #	La	Ce	Nd	Sm	Eu	Dy	Er	Yb
13-4	0.18	0.27	0.46	0.58	0.37	0.59	0.51	0.50
13-1/2	0.25	0.37	0.56	0.57	0.31	0.72	0.75	0.79
13-3	0.11	0.17	0.31	0.44	0.31	0.53	0.44	0.50
average 13	0.18	0.27	0.44	0.53	0.33	0.61	0.57	0.60
19A-1	0.07	0.11	0.23	0.38	0.28	0.42	0.33	0.35
9-1	0.03	0.05	0.12	0.21	0.16	0.26	0.19	0.21

Table DIV Comparable partition coefficients from the literature

Reference	La	Ce	Nd	Sm	Eu	Dy	Er	Yb
Villemant et al. 1981	0.12	-	-	-	0.63	-	-	-
Dostal et al. 1983	0.14	0.19	-	0.8	0.55	-	-	0.65
Grutzeck et al. 1974	0.069	0.98	0.21	0.26	0.31	0.33	0.3	-
Nicholls & Hart 1980	0.14	-	-	0.5	-	-	-	0.9
Philpotts & Schnetzler 1970	-	0.08	0.17	0.26	0.27	0.35	0.33	0.29

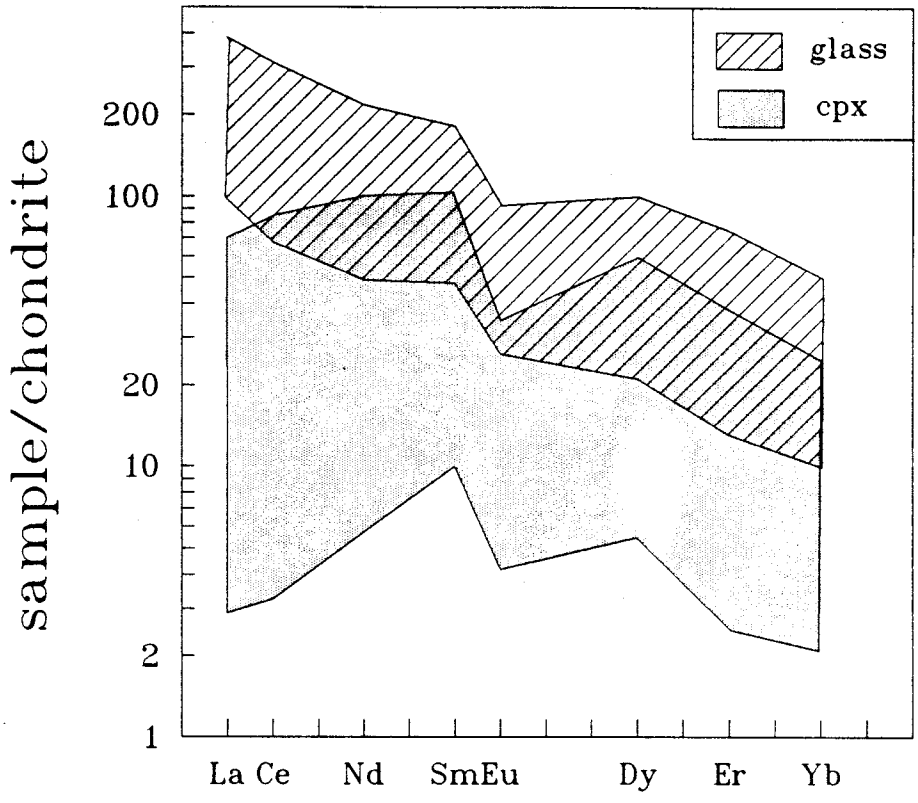

Fig. D1: REE pattern of selected glass and clinopyroxene in sample #9, #13 and #19A, analyzed on the ion-microprobe.

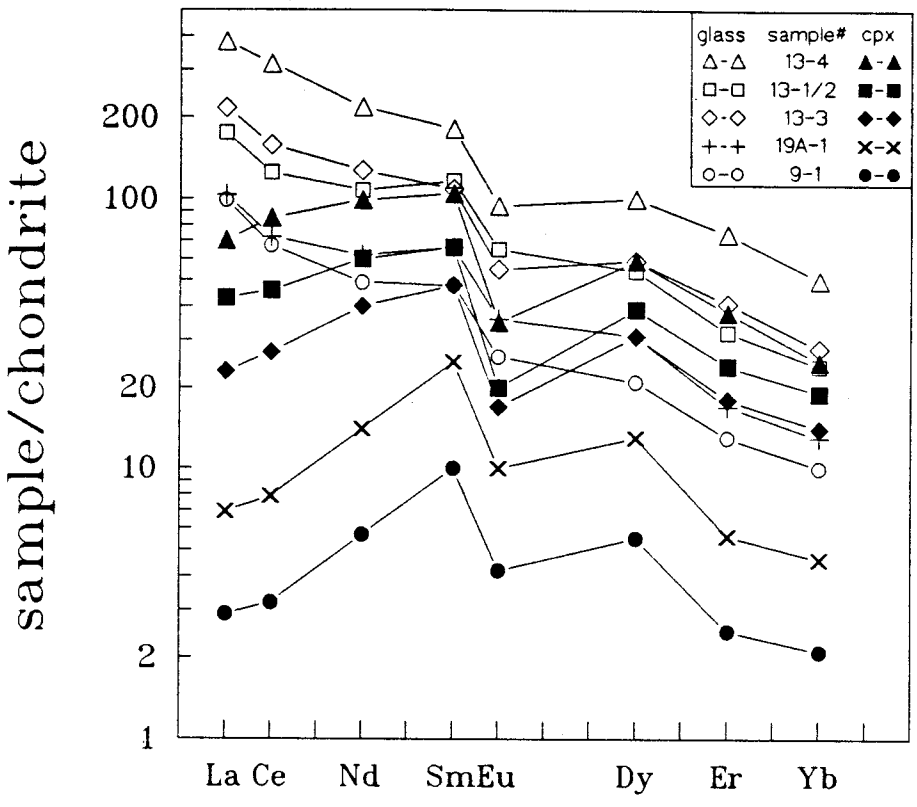

Fig. D2: REE pattern of glass and clinopyroxene for single runs of sample #9, #13 and #19A on the ion-microprobe.

According to these ion microprobe analyses, equilibrium between glass and cpx for both trace elements and REE points towards a true "trapped origin" for the liquid phase in the gabbro. Partition coefficients from the ion microprobe that are one of the major factors of uncertainty in the model have similar values when compared to the ones used in the model. However, trace element concentrations of incompatible elements are still very high and seem to be an ongoing controversial factor in the discussion whether the host hawaiitic rock is responsible for the glass phase or whether it is true trapped liquid.

References for appendix D

Dostal, J., Dupuy, C., Carron, J. P., LeGuenDeKerneizon, M. and Maury, R. C. (1983) Partition coefficients of trace elements: application to volcanic rocks of St. Vincent, West Indies. Geochim. Cosmochim. Act. 47, 525 - 533.

Grutzeck, M. Kridelbaugh, S. and Weill, D. (1974) The distribution of Sr and REE between diopside and silicate liquid. Geophys. Res. Lett. 1, 273 - 275.

Johnson, K. T. M., Dick, H. J. B. and Shimizu, N. (1990) Melting in the oceanic upper mantle: an ion microprobe study of dioside in abyssal peridotites. J. Geophys. Res. 95, 2661 - 2678.

Nicholls, I. A. and Harris, K. L. (1980) Experimental REE partition coefficients for garnet, clinopyroxene and amphibole coexisting with andesitic and basaltic liquid. Geochim. Cosmochim. Act. 44, 287 - 308.

Philpotts, J. A. and Schnetzler, C. C. (1970) Partition coefficients of rare earth elements between igneous matrix and rockforming mineral phenocrysts II. Geochim. Cosmochim. Act. 34, 331 - 340.

Villemant, B., Jaffrezic, H., Joron, J.-J. and Treuil, M. (1981) Distribution coefficints of major and trace elements; fractional crystallization in the alkali basalt series of Chaîne des Puys (Massif Central, France). Geochim. Cosmochim. Act. 45, 1997 - 2016.